CHARACTERIZING MIST FLOW IN MINIMUM QUANTITY LUBRICATION DRILLS

A Thesis

by

JAY KAMLESH RAVAL

Submitted to the Office of Graduate and Professional Studies of
Texas A&M University
in partial fulfillment of the requirements for the degree of

MASTER OF SCIENCE

Chair of Committee,	Bruce Tai
Committee Members,	Wayne Hung
	Satish Bukkapatnam
Head of Department,	Andreas Polycarpou

August 2019

Major Subject: Mechanical Engineering

Copyright 2019 Jay Kamlesh Raval

ABSTRACT

Minimum Quantity Lubrication (MQL) uses a mixture of oil and air in small quantities to effectively lubricate and cool the cutting zone. Because of this small quantities of lubricants being used in the order of 5-100 ml/hr., the control of the flow is a critical parameter. Presently, this control is done by multiple experimentation to find out the optimal conditions. This method though works does not provide enough insight on how each parameter affects the effectiveness of the MQL. Moreover, the flow in MQL is a multiphase flow and thus the distribution of the lubricant might not be homogeneous as expected. A new method is proposed in this article to capture and analyze the flow distribution in through channel drills employing MQL using visible light. The amount of light reflected by the mist particles works as a signal to quantify the amount of mist particles at particular location. Image acquisition at multiple viewing angles was carried out to map flow across channel cross-section. The measurement and analysis process provides data about flow concentration zones in the channel, which help in the design of better cutting tools. The effect of channel shape and the helix angle of the cutting tool; (which controls the helix angle of the channel) on the flow distribution obtained were analyzed. The flow distribution results at the channel exit were compared to the velocity contours at the same location, obtained using CFD simulation, to find out analogy in the flow velocity and flow distribution.

ACKNOWLEDGEMENTS

I would like to thank my committee chair, Dr. Tai and my committee members, Dr. Hung and Dr. Bukkapatnam for their guidance and support throughout the course of this research.

Thanks also goes to my friends, colleagues and department faculty and staff for making my time at Texas A&M University a great experience.

Lastly, thanks to my family for their constant support, motivation and love throughout my graduate studies.

CONTRIBUTORS AND FUNDING SOURCES

Contributors

This work was supervised by a thesis committee consisting of Asst. Prof. Dr. Bruce Tai (Advisor) of the Department of Mechanical Engineering, Assoc. Prof Dr. Wayne Hung of the Department of Engineering Technology and Industrial Distribution and Prof. Satish Bukkapatnam of the Department of Industrial and Systems Engineering.

The velocity measurement data used to perform the CFD study was provided by Dr. Stephenson from Ford Motor Company (Dearborn, MI) and the dual channel MQL system used for the experimentation was facilitated by Mr. Walker from UNIST (Grand Rapids, MI). I would also like to thank Dr. Charoenphol for providing micropipette for sessile drop measurements.

All other work related to the thesis was conducted by the student independently.

Funding Sources

This study was supported by funding provided by NSF grant #1760985. Its contents are solely the responsibility of the authors and do not necessarily represent the official views of the NSF.

TABLE OF CONTENTS

Page

ABSTRACT……...ii

ACKNOWLEDGEMENTS……..iii

CONTRIBUTORS AND FUNDING SOURCES……iv

TABLE OF CONTENTS……...v

LIST OF FIGURES……vii

LIST OF TABLES……ix

1. INTRODUCTION……1

1.1. Motivation……..1
1.2. Literature Survey ……..……...……..3
1.3. Research Scope ……..……...10

2. EXPERIMENTAL SETUP, MATERIALS AND METHODS……..12

2.1. Experimental Setup……..12
2.2. Image Acquisition and Processing.....17

3. EXPERIMENTAL RESULTS……25

3.1. Design of Experiments……25
3.2. 0° Helix Angle Circular Channel……27
3.2.1. Results for 0°, 45° and 90° Viewing Angle ……..27
3.2.2. Flow Mapping Using the Normalized Profiles ……...32
3.3. Results for 30° and 45° Helix Angle Circular Channel ……..33
3.4. Results for Triangular Channels ……35
3.5. 0° Helix Angle Reversed Triangular Channel ……39

4. NUMERICAL SOLUTION……....41

4.1. CFD Model Setup and Boundary Conditions ……41
4.2. Computational Results……43
4.2.1. Solution for Circular Channels ……43
4.2.2. Solution for Triangular Channels……45
4.2.3. 0° Helix Angle Reversed Triangular Channel ……47

Page

4.3. Comparison of the Results ……...47

5. DISCUSSION, CONCLUSIONS AND FUTURE SCOPE …….....49

5.1. Discussion ……....49
5.2. Conclusions……..51
5.3. Future Scope ……51

REFERENCES ……53

LIST OF FIGURES

Page

Figure 1: Heat generation in metal cutting ……1

Figure 2: Classification of MQL systems ……..4

Figure 3: Types of MQL systems ……..5

Figure 4: Types of multiphase flow...……8

Figure 5: Multiphase flow measurement methods…….9

Figure 6: Experimental setup for simulating the flow in through tool channels in drill bits……12

Figure 7: Forces acting on stationary liquid droplet ……14

Figure 8: Sample image for contact angle measurement…….15

Figure 9: Image acquisition using optical light and a CCD camera ……18

Figure 10: Concepts behind proposed method ……19

Figure 11: Effect of observation plane on the channel exit shape ……...20

Figure 12: Investigation of irradiance on the flow distribution……...22

Figure 13: Generation of ideal profile for homogeneous dispersed/mist flow ……23

Figure 14: Radon transform…….24

Figure 15: Change in the helix angle of the drill and the helical channel ……...26

Figure 16: Viewing angles used to capture the flow from multiple angles …….27

Figure 17: Position an orientation of camera for different viewing angles …….28

Figure 18: Step by step image processing for 0° helix angle circular channel drill at 0° viewing angle……...30

Figure 19: Normalized profiles for 0° helix angle circular channel ……31

Page

Figure 20: Mapping the projections back on the exit area……..32

Figure 21: Results for 30° helix angle circular channel ……..33

Figure 22: Results for 45° helix angle circular channel……...35

Figure 23: Results for 0° helix angle triangular channel ……36

Figure 24: Results for 30° helix angle triangular channel ……...37

Figure 25: Results for 45° helix angle triangular channel ……...39

Figure 26: Results for 0° helix angle reversed triangular channel……...40

Figure 27: Control volume for simulation ……...42

Figure 28: Velocity contours at exit for 0° helix angle circular channel…….43

Figure 29: Velocity contours at exit for 30° helix angle circular channel……...44

Figure 30: Velocity contours at exit for 45° helix angle circular channel……...44

Figure 31: Velocity contours at exit for 0° helix angle triangular channel …….45

Figure 32: Velocity contours at exit for 30° helix angle triangular channel……46

Figure 33: Velocity contours at exit for 45° helix angle triangular channel……46

Figure 34: Velocity contours at exit for 0° helix angle reversed triangular channel…...47

LIST OF TABLES

Page

Table 1: Measured values of contact angle of UNIST Coolube 2210 with Formlabs clear material……16

Table 2: Design of experiments ……25

Table 3: Comparison of experimental results and numerical solution ……48

1. INTRODUCTION

1.1. Motivation

Today's human lifestyle includes a lot of engineered products which help in improving the standard of living. Ranging from a small needle to large automobiles, these products facilitate the user to complete important as well as mundane tasks. A lot of thought and effort is required behind the design of these products which led to concepts like Design for Manufacturability (DFM) and Design for Excellence (DFE) to name a few. The manufacturing of product can be carried out either using subtractive processes or by using additive processes.

The subtractive processes or machining processes can be used to manufacture metal as well as non-metals. With the help of numerical control machines they can be used to produce complex shapes with tight tolerances. The relative motion between the tool and the workpiece induces shear stress on the workpiece, this shear stress plastically deforms the material and later separates it in the form of chips. Because of this plastic deformation and friction, heat is generated at the tool-workpiece contact zone as can be seen in fig. 1.

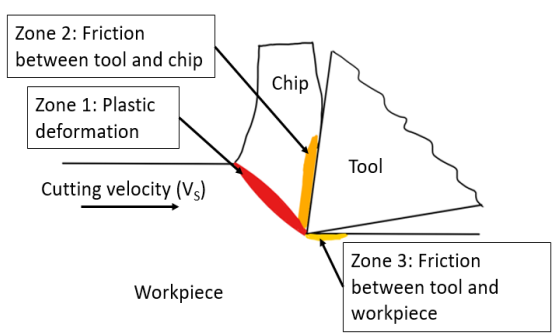

Figure 1: Heat generation in metal cutting.

This heat reduces the hardness of the tool and also reduces the tolerances of the process because of thermal expansion and contraction. Therefore, cutting fluids are applied during the cutting to mitigate the effects of friction and high temperature. When the cutting interface if flooded with cutting fluids with the primary motive to reduce the temperature, it is called flood cooling. According to a survey conducted by Jost machinery, cutting fluids incur about 10-15% of the total machining costs. Thus, dry cutting or near dry cutting like MQL can reduce the total machining costs by the same amount. MQL also known as near dry machining, uses a small quantity of lubricant sprayed directly at the cutting interface in the form of mist to reduce the amount of heat generated and lower the temperature. This method is advantageous over flood cooling because, it does not require any recirculation or filtration system. Therefore, in recent years MQL is gaining popularity in the manufacturing industry. With the use of special tooling MQL can be applied to all the machining processes.

Turning and milling have easily accessible cutting zone and thus can use externally applied MQL. On the other hand, drilling has low accessibility to the cutting zone and thus, drills with through-tool channels are required to efficiently apply the cutting fluids. There have been multiple studies which analyze the effect of MQL parameters like pressure, flow rate, lubricant concentration etc. on the effectiveness of MQL. However, limited amount of data is available about the flow structure characterization which controls the distribution of lubricant on the surface. Moreover, the currently available multiphase flow characterization methods are inefficient in measuring MQL flow.

1.2. Literature Survey

The manufacturing processes can be broadly classified into additive manufacturing processes and subtractive manufacturing processes. The additive manufacturing processes provide more flexibility in the complexity of shapes that can be produced but they are limited by the mechanical properties produced and the tolerances required. Therefore, usually additive manufacturing processes need some form of post processing[1]. Because of the above reasons, majority of the products go through some subtractive manufacturing/machining process. The plastic deformation of the material and the rubbing of the chips and tool generates thermal energy at the cutting zone. This thermal energy increases the temperature of the tool and workpiece, which increase tool wear, Built-up Edge (BUE) formation and tool failure, these effects lead to reduction in tool life [2, 3]. To mitigate this effect, cutting fluids are used.

Cutting fluid can be applied either by flood cooling or by MQL. The flood cooling technique uses large quantities if water based coolant mixed with additives to enhance the performance. However, there is a need of recirculation and filtration system to be able to use the coolant for longer periods. The water in the coolant also increases chances of rusting on the machine tool which reduce the life of the machine. Furthermore, the lubricants or coolants used in flood cooling expose workers to disorders like asthma, pneumonia, acne, skin irritation and sometimes even skin cancer[4]. However, the extent of these effects is dependent on the type of coolant/lubricant used and but generally mineral oils are more harmful compared to vegetable oils. These problems can be tackled if MQL is used. MQL uses a small quantity of cutting fluid (usually vegetable

based/biodegradable) to lubricate the cutting zones. As its name implies, the amount of cutting fluid used in MQL is very low and thus no recirculation and filtration systems are required on the machine. Moreover, there are been studies comparing the performance of MQL and dry and flood cooling. It has been proven that MQL is capable of providing longer tool life, better surface finish and better dimensional control [5-9]. Moreover, the parts produced using MQL are dry and thus ready to be used for the next process without the need of cleaning. Considering the above advantages, MQL is a better option as compared to flood cooling.

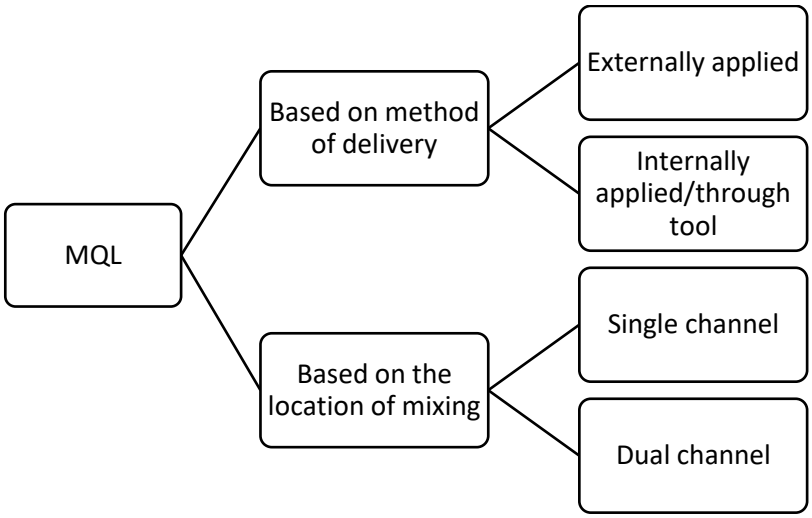

Figure 2: Classification of MQL systems.

As can be seen in fig. 2 that MQL systems can be either classified based upon the method of delivery of the lubricant or based upon the location of mixing. The externally applied MQL system (as seen in fig. 3(c)) uses a nozzle that is pointed towards the cutting zone to deliver the lubricant. The internally applied MQL system (as seen in fig. 3(b)) use specially designed tools which have through channels to deliver the lubricant. The

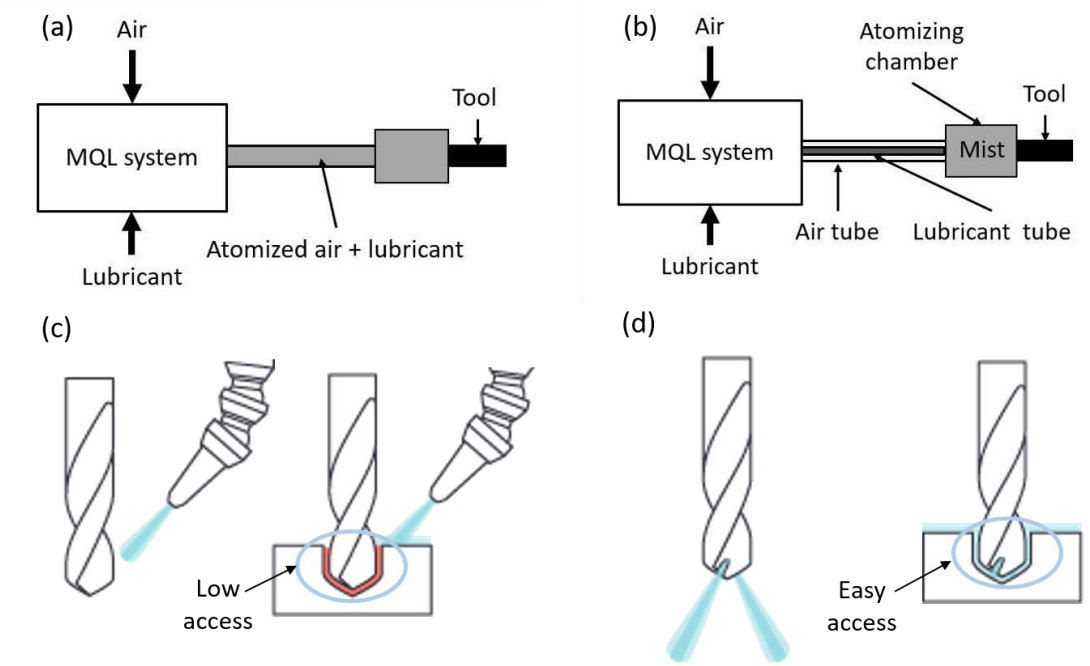

Figure 3: Types of MQL systems. (a) Single channel MQL system (b) Dual channel MQL system (c) Externally applied MQL system (d) Internally applied/through tool MQL system

externally applied systems are usually used for turning, milling operations because they are easily accessible and thus no special tools are required. However, for processes like drilling and boring, the cutting zone is not easily accessible and thus the internally applied MQL systems work better[10]. MQL uses pressurized air to create mist and deliver it to the cutting zone. Based upon the location of mist generation MQL systems can be classified into two categories single channel (as seen in fig. 3(a)) and dual channel (as seen in fig. 3(b)). In the single channel systems, the mist is made in an atomizing chamber near the MQL system and then transferred to the cutting zone using a single tube. The dual channel systems transfer the pressurized air a lubricant in separate channels (usually concentric) and then the mist is atomized near the cutting zone and delivered. The mist produced using single channel systems tend to have larger droplet size as compared to the

dual channel systems. The reason being that the small droplets coagulate during their transfer from the system to the cutting zone, this problem is not encountered in the dual channel systems because the mist is generated right before the delivery.

A dual channel internally applied MQL system is the best option for application in drilling process because, the lubricant can be delivered to the cutting zone even during deep hole drilling maintaining smaller droplet size. The amount of lubricant being used in MQL is low and thus effective delivery of the lubricant is important for the process to be beneficial. According to the study by Kuzu et al.[11] the heat generation in the drilling operation is not uniform across the cutting edge of the drill bit and thus small deviation in the flow distribution can change the quality of the product obtained [12]. Thus, there is a need to control the distribution of lubricant on the cutting edge.

Plenty of research has been conducted on MQL flow. Most of the research is experimental research where the effect of machining parameters and MQL parameters is investigated on the machining quality obtained. Tawakoli et al. investigated the effect of MQL parameters like oil flow rate, air pressure, MQL nozzle position and distance from the cutting zone. They found out that all these parameters do affect the machining quality[13]. In another study Davim et al. investigated the effect of feed, cutting power on the surface roughness and concluded that with the selection of proper parameters results equivalent to flood cooling can be obtained[14]. Attanasio et al. compared the tool life obtained using MQL and flood cooling, they concluded that both MQL and flood cooling provide similar tool life, but the MQL process is more efficient if the nozzle is pointed on the flank face[15]. There have been plenty of other studies which study the above

mentioned parameters and all of them conclude, MQL to be at least as efficient as flood cooling and having the potential to provide even better results if properly set up [16-19].

There have also been studies to characterize the MQL flow where the droplet size or velocity field have been studied. Khan et al. measured the droplet size and successfully measured droplet sizes as small as 5μm and also concluded that higher pressure c=values can generate smaller droplet size[20]. Rahim et al. also measured the droplet size for different diameter nozzle and found out that tiny droplet from MQL provide better lubrication effect and thus increase the efficiency of the process[21]. Sovani et al. investigated the effect of pressure on the mist generated and also on the cone angle formed at the exit[22]. Husted et al. performed PIV and PDA on high pressure water mist and they found out that both the systems have problem measuring the properties near the exit because of high flow density and fast speeds[23]. In another study Park et al. studied the droplets and their distribution for minimum quantity lubrication[24].

Therefore it is evident that limited amount of data is available for flow characterization in MQL. Reason being, the measurement of properties of multiphase flow is not as simple as single phase flow. The estimation of properties of multiphase is difficult because the properties of multiphase cannot be directly found by combining the properties of its single phase components. Multiphase flow is characterized based upon the distribution of its phases in the fluid. Fig. 4 shows the types of multiphase flow[25]. The distribution of the phases is based upon the relative velocity and relative mass concentration.

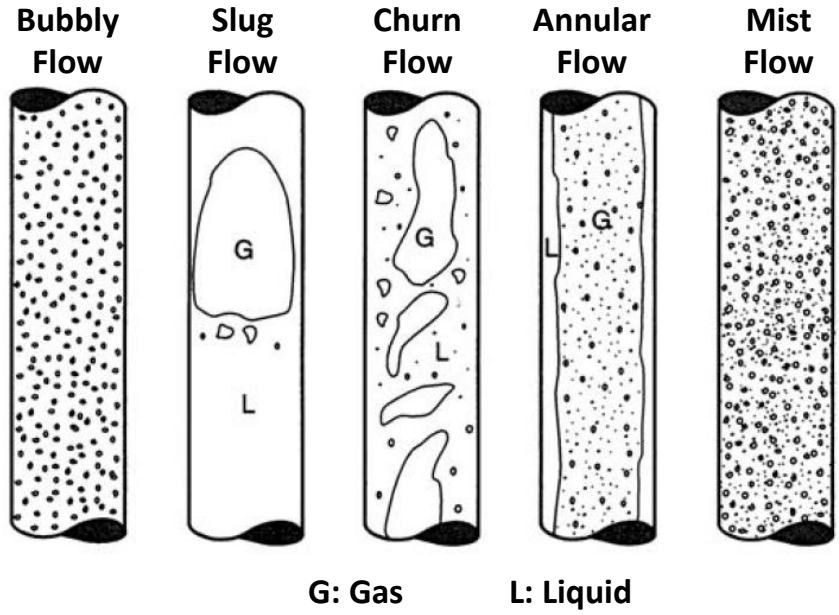

Figure 4: Types of multiphase flow.

Since MQL is a multiphase flow, there are multiple methods already available to characterize multiphase flow. The methods can be classified into two categories namely invasive methods and non-invasive methods. The invasive methods require a probe or other sensor to be inserted in the flow channel to measure the properties of the flow. These methods can measure the local as well as average properties. Some common invasive methods include hot wire anemometry, Multiphase flow meters (MPFMs). The invasive method measuring equipment usually need to be installed into the flow passage to be able to get results. Therefore, for the case of through tool channels, where the channel size is of the order of 1-2 mm, the invasive measurement methods will disrupt the flow considerably and thus the results obtained will not be accurate. Some common invasive multiphase flow measurement methods are shown in fig. 5(a) and 5(c).

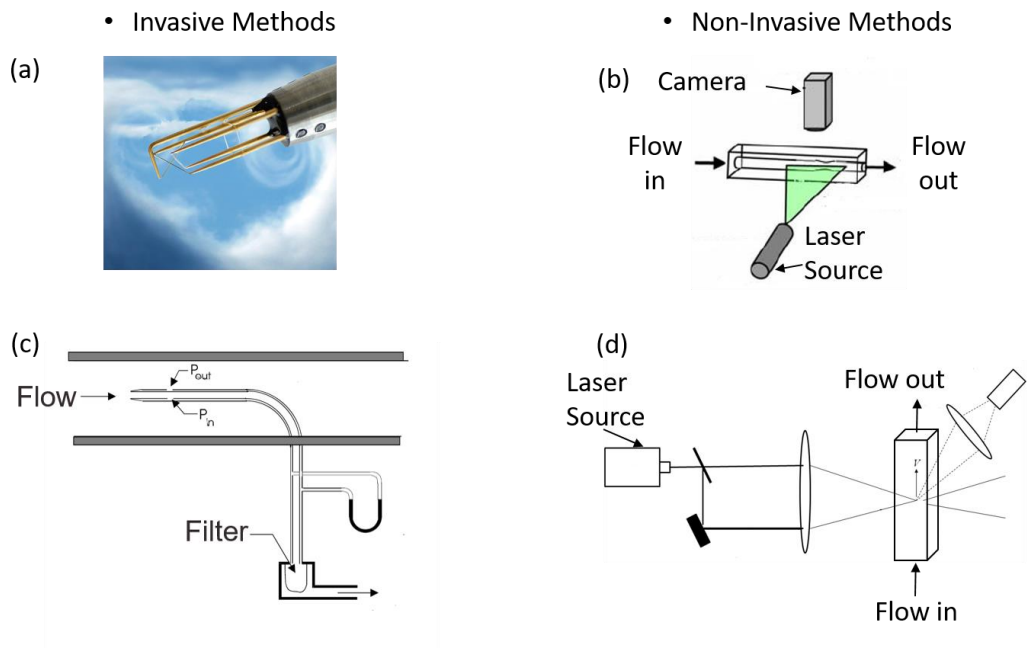

Figure 5: Multiphase flow measurement methods. (a) Hot wire anemometer (b) Particle Image Velocimetry (PIV) (c) Isokinetic sampling (d) Phase Doppler Anemometry (PDA)

The non-invasive methods have the advantage of being able to measure the flow without disrupting it therefore, they have been widely used in the industry. However, this advantage comes with the need of extra computational power. Particle Image Velocimetry (PIV), Phase Doppler Anemometry (PDA), Optical Coherence Interferometry (OPI), Magnetic Resonance Imaging (MRI), Neutron and X-Ray Image Velocimetry etc. PIV and PDA are particle tracking methods. In a 3D flow, a plane is illuminated using a pulsed LASER which is synchronized with the image capturing camera. The pulse of LASER is in the order of picosecond, and thus high speed image acquisition methods are required for the process to work. High speed image acquisition requires high intensity light in order to be able to capture the flow because of short frame exposure time. For the case of MQL

in through tool channels of drill, the average velocity of particles in the channel is in the order of 100 m/sec [26, 27]. This extremely high speed of the droplet makes the measurement of velocity using PIV and PDA nearly impossible. Moreover, because of the helical channel, the flow of the droplets is not planar and thus there is a high chance of tracking particles leaving the illuminated layer leading to loss of data. Because of the above reasons PIV and PDA techniques are inefficient in measuring this kind of flow. MRI technology uses a strong magnetic field to align the protons, the change in the magnetic field is measured which works as a signal for the technique. This technique mostly depends on the excitation to the water molecules due to the magnetic field, this cannot be applied to MQL as the fluid does not have any water. Moreover, the machinery used is made of metal which can disrupt the magnetic field and thus it is not suitable for this particular application. Neutron and X-ray imaging use respective waves which travel through the flow and are absorbed by the flow. The attenuation of the intensity of the signal works as a signal for the measurement. These techniques use hazardous rays and thus are not suitable for MQL flow characterization.

1.3. Research Scope

The limited amount of data available in characterizing the MQL flow in through tool channels leads to need for a measurement method capable of measuring the flow distribution. The following are the objectives of this study:

1. Propose a new method to characterize multi-phase flow distribution in through-tool channels employing MQL.

2. Using the proposed method to investigate the effect of design parameters on the multi-phase flow distribution.

3. Perform simulations to find the single phase velocity profile at the channel exit area.

4. Compare the multi-phase flow distribution with the single phase velocity profile and conclude for any correlation.

2. EXPERIMENTAL SETUP, MATERIALS AND METHODS

2.1. Experimental Setup

The objective of the study was to find the flow distribution in through tool channels in MQL drilling. After the literature survey it was found that the channel need to be easily accessible by the sensors to be able to efficiently measure the multiphase flow distribution. After multiple experiments it was decided the use slow motion imaging to capture the flow distribution. The design of the setup was to be such that it would allow easy alignment of the drill bit w.r.t the camera. Thus extrusion channels were used to create the structure of the setup since they allow easy modifications. Fig. 6 shows the lab scale experimental setup designed at developed during the study.

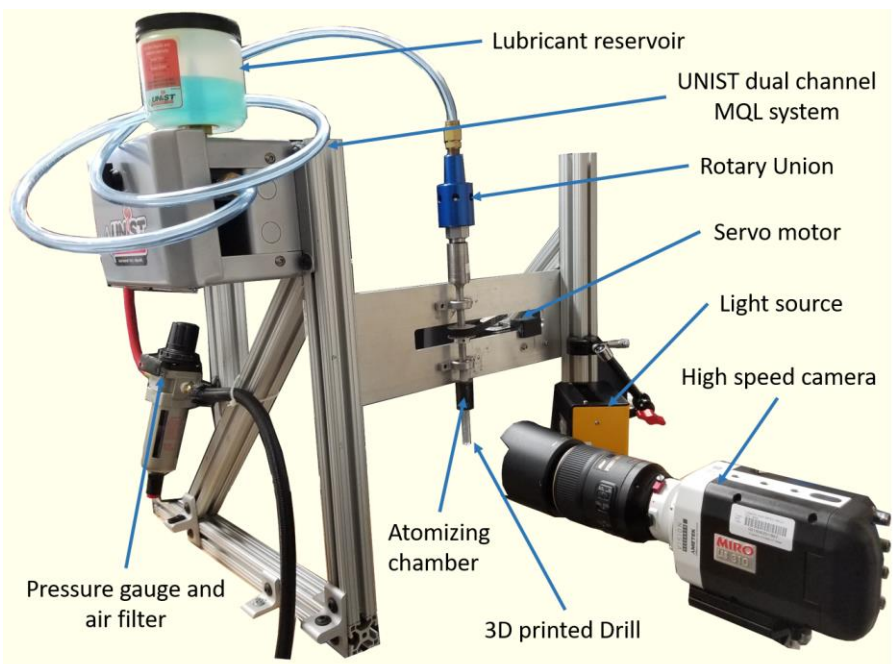

Figure 6: Experimental setup for simulating the flow in through tool channels in drill bits.

The system shown in the figure consists of a dual channel MQL system (Coolubricator™, UNIST Inc., Grand Rapids, MI). The system uses two concentric channels to deliver the air and lubricant to the tool. The tube for air encapsulates the tube for lubricant. The pressurized air is supplied to the system at a constant value of 50 psi through an air filter to remove any form of impurities. The lubricant used for the process is UNIST Coolube 2210, which was developed by UNIST specifically for non-ferrous metal cutting, which had intermediate values for surface tension and viscosity among commonly used MQL lubricants[27]. MQL flow rate varies between 5 ml/hr. to 50ml/hr. in the operating conditions based upon the cutting parameters. For better visualization purposes the flow rate was kept constant at 40 ml/hr.

Because an internal channel system was used, there was a need of a rotary union to connect the spindle and the tubing. The rotary union allowed the spindle and the shaft to rotate freely without rotating the tubes used to deliver the fluids. A servo motor is connected to the shaft using a pulley and timing belt arrangement. The servo motor allowed control over the rotation speed as well as the rotation angle. For image acquisition Phantom Miro lab310 a high speed camera capable of capturing 3200 (frames/sec) fps greyscale images of resolution 1200 × 800 pixels was used. Along with it, a Nikon lens with a focal length of 105 mm and a maximum aperture of f/2.8.

The motive of the study is to study the flow structure for multiple drills. Therefore, since the drill bits were not going to actually cut the workpiece and also to facilitate fast and easy modification, 3D printing technology was used to design and manufacture the drill bits. This allowed flexibility in the design process as customizing 3D printed drills is

cheaper and faster as compared to carbide drills. Out of all the available 3D printing technologies, Stereolithography (SLA) was chosen because of the high printing resolution and wide availability of materials. Formlabs (Somerville, MA) Form 2 with a resolution of at-least 100µm was used to manufacture the drills. This allowed fine surface finish and precise geometry control. Because the mist has a high surface to volume ratio, the adhesion forces play a critical role in the behaviour of mist in channels. Since, the material used for printing is a propriety material by Formlabs (Formlabs Clear) which is different than the common cutting tool material (WC), the interaction of the mist with the proprietary material needs to be verified to be similar to the WC. The adhesion forces can be investigated by measuring the contact angle. There are multiple methods to measure contact angle, out of which sessile drop method was used to measure the contact angle of UNIST Coolube 2210 with clear material of Formlabs. The contact angle of a drop is governed by Young's equation as shown in the fig. 7.

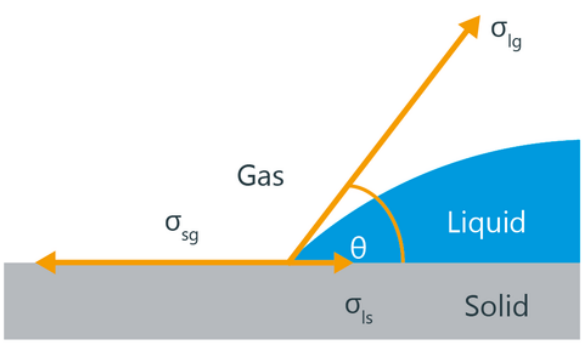

σ_{sg} = solid gas interfacial energy

σ_{ls} = liquid solid interfacial energy

σ_{lg} = liquid gas interfacial energy

θ = contact angle

$$\sigma_{sg} - \sigma_{ls} - \sigma_{lg} * \cos\theta = 0$$

"Young's Equation"

Figure 7: Forces acting on stationary liquid droplet.

As can be seen in the figure, there is a force acting on every interface. The Young's equation is the equation obtained using force balance. A higher value of contact angle means higher surface tension or surface free energy. And a lower value of contact angle means low free surface energy. A higher surface energy allows for higher adhesion forces and thus reduces the contact angle. The contact angles of standard cutting fluids with standard tools was measured by Lerma et al. and Tai et al.[7, 27]. The contact angle of Coolube 2210 with WC tool ranged from 10° - 18°. For measurement of contact angle, sessile drop method was used. A sample plate was printed using the From 2 printer. The printing orientation of the sample plate was kept same as the printing orientation of the drills. This was done to ensure that the measurement can give a fair comparison with the drills knowing the fact that the 3D printed parts are highly anisotropic. The contact angle of Formlabs Clear material with Coolube 2210 ranged from 15° - 17° as can be seen in fig 8 and table 1. These values aligned with the measured values of contact angle in the literature and thus it was assumed that, the lubricant interaction with WC and Formlabs clear material is similar.

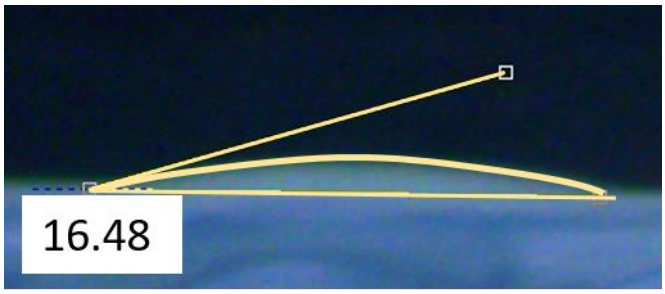

Figure 8: Sample image for contact angle measurement.

Sr. No.	Contact angle
1	16.48
2	17.73
3	16.16
4	17.34

Table 1: Measured values of contact angle of UNIST Coolube 2210 with Formlabs clear material

The small values of contact angle means good wettability of the lubricant. This makes sense because the lubricant is specifically designed to adhere with the workpiece and create layer to reduce friction. The high wettability and low viscosity of the lubricant allows deeper penetration to the cutting zone, and thus can provide better efficiency in cutting. Moreover, the surface roughness also affects the value of contact angle but the effect was considered for this study.

After confirming that the interaction of the droplets with the Formlabs Clear material is similar to that with WC, the experiments were started. Dasch and Kurgin characterized the mist generated in MQL and conducted experiments to find the effect of rotating velocity of the tool on the mist flow rate[28]. They found out that the rotating speed of the tool has minimal influence on the mist flow rate. Moreover, the due to the substantial velocity difference between the tangential direction and the axial direction, the flow patterns produced at stationary condition should be similar to that produced at rotating conditions. This assumption is supported by the results obtained by Yamamoto et al. who simulated the flow through a helical coil with a circular cross-section[29]. They concluded that the results in the velocity contours is independent of the rotation of the drill. Image

acquisition was carried out a three different angles across the axis of the tool to better understand the distribution of mist across the area of the channel. The viewing angles are named based upon the angle of rotation of the drill on its axis of rotation. A 0° viewing angle means the chisel edge is exactly parallel to the camera and a 90° viewing angle means that the chisel edge is exactly perpendicular to the camera. The 45° viewing angle is the obtained when the drill is rotated by 45° along its axis. Considering all of these conclusions, the experimental setup was designed as shown in fig. 6.

2.2. Image Acquisition and Processing

As explained in the literature survey section, there is no efficient method to measure the mist flow distribution in cases like MQL. Therefore, a new method to analyze the flow distribution is proposed in this section.

MQL is a gas-liquid multiphase flow, therefore whenever optical viewing techniques are used to capture the flow only the liquid droplets will be captured. Since air is transparent and will reflect no light in to the camera. This can be used as an advantage to filter out the distribution of lubricant from the overall flow. The interaction of light is complicated because the liquid droplets do reflect light but also allow light to transmit through them. In other words liquid droplets are translucent and they attenuate the amount of light energy passing through them. Also, there are effects like light scattering and absorption. All these losses can be neglected if the intensity of light source is high enough to increase the contrast and reduce attenuation loss.

The liquid droplets will reflect the light into the camera and the amount of light entering the camera is proportional to the no of droplets. Since the flow is in 3D the image

captured will be a superposition of flow in multiple planes at different depths. Fig. 9 shows how the camera captures the fluid flow. It explains how a 3D control volume is discretized into multiplanes at different depths and also how light passes through each plane to create a superimposed image as seen in bottom right corner of fig. 9.

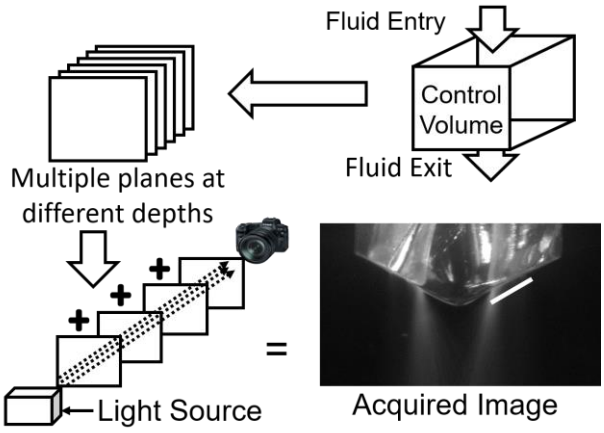

Figure 9: Image acquisition using optical light and a CCD camera.

To allow the camera to focus at multiple planes at once the principle of deeper depth of field is used. Fig. 10 shows a schematic explaining the correlation between the aperture and the depth of field. A deeper depth of field means the camera has a sharp image in a thicker region and a shallow depth of field means the camera is focused on a thin region.

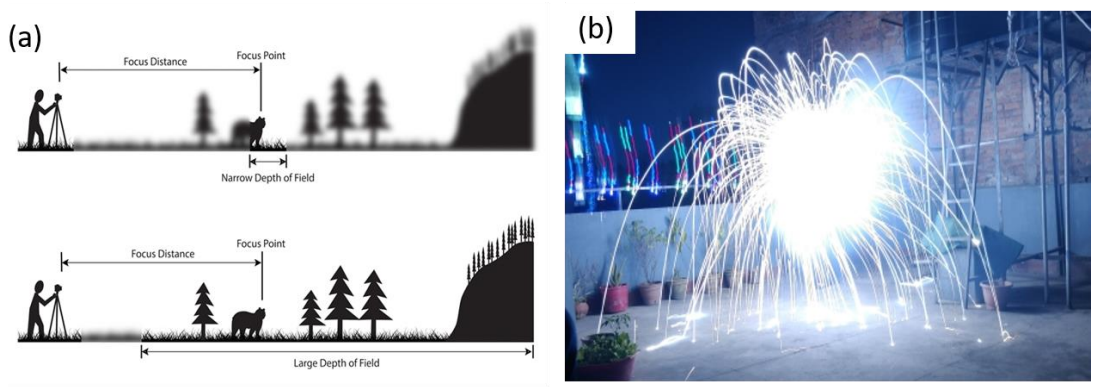

Figure 10: Concepts behind proposed method. (a) Effect of aperture on depth of field (b) Effect of exposure on the image captured

As can be seen in the figure, a smaller aperture can provide a deeper depth of field. However, a smaller aperture means that the amount of light going inside the camera is reduced and thus a brighter light source is required to capture bright enough images. To handle this reduction in the amount of light entering the sensor, the exposure time of the camera has been increased so that each frame is exposed for a longer amount of time and thus the image has sufficient intensity.

The exit of the channel works as a nozzle and thus the flow expands as soon as it leaves the channel. The flow measurement should be done as close to the channel as possible to avoid the expansion of the flow. Therefore the image intensity should be measured along the highlighted line shown in bottom right of fig. 9. This mitigates the effect of flow expansion into the measurement data. Fig. 11 shows the channel geometry obtained when the highlighted line is perpendicular to the axis of rotation vs when the highlighted line is parallel to the exit area for a circular coolant channel in a drill without any helix angle. The projection perpendicular to the axis of drill gives a circle while the projection parallel

to the exit area gives an ellipse. Thus the line along which an ellipse is obtained was chosen for plotting the intensity of the pixels.

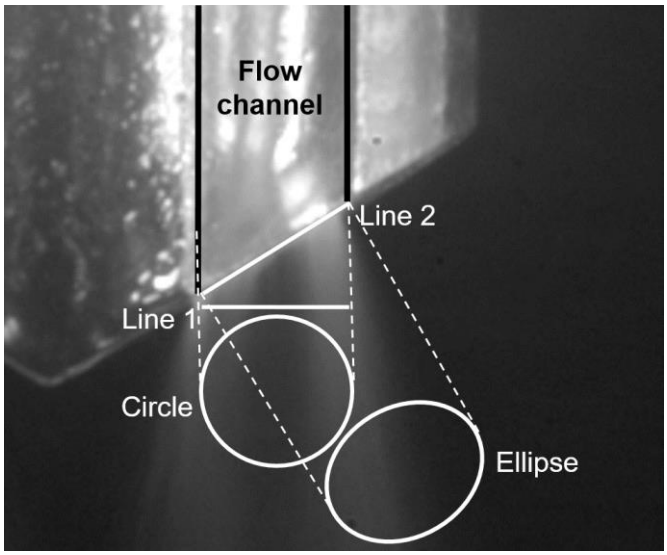

Figure 11: Effect of observation plane on the channel exit shape.

Thus, the line 2 highlighted in fig. 11 is the plane along which the flow characterization will be performed. The schematic of image acquisition is shown in the fig. 9. Top right corner shows the control volume and the direction of fluid flow. The top left corner shows the discretization of a volume as a combination of multiple planes. Because of the deeper depth of field all of these planes are in focus. As can be seen in the bottom left corner the light is reflected from all the planes and then enters in the camera. The bottom right image is a sample image captured using the technique. As can be seen that the intensity of flow is not the same at all the locations across the channel. This is because the flow distribution is not the same at all the locations.

The intensity of the pixel is proportional to the amount of light reflected along the line perpendicular to the pixel. And the amount of light is proportional to the density of lubricant at a particular location. Therefore, the intensity of the pixel is proportional to the density of the lubricant. On a 2D image the intensity of pixels along a line will represent the distribution of mass flow rate through a plane passing through the reference line and perpendicular to viewing angle. The irradiance (amount of light entering the control volume) was investigated to find out the effect of irradiance level on the profile

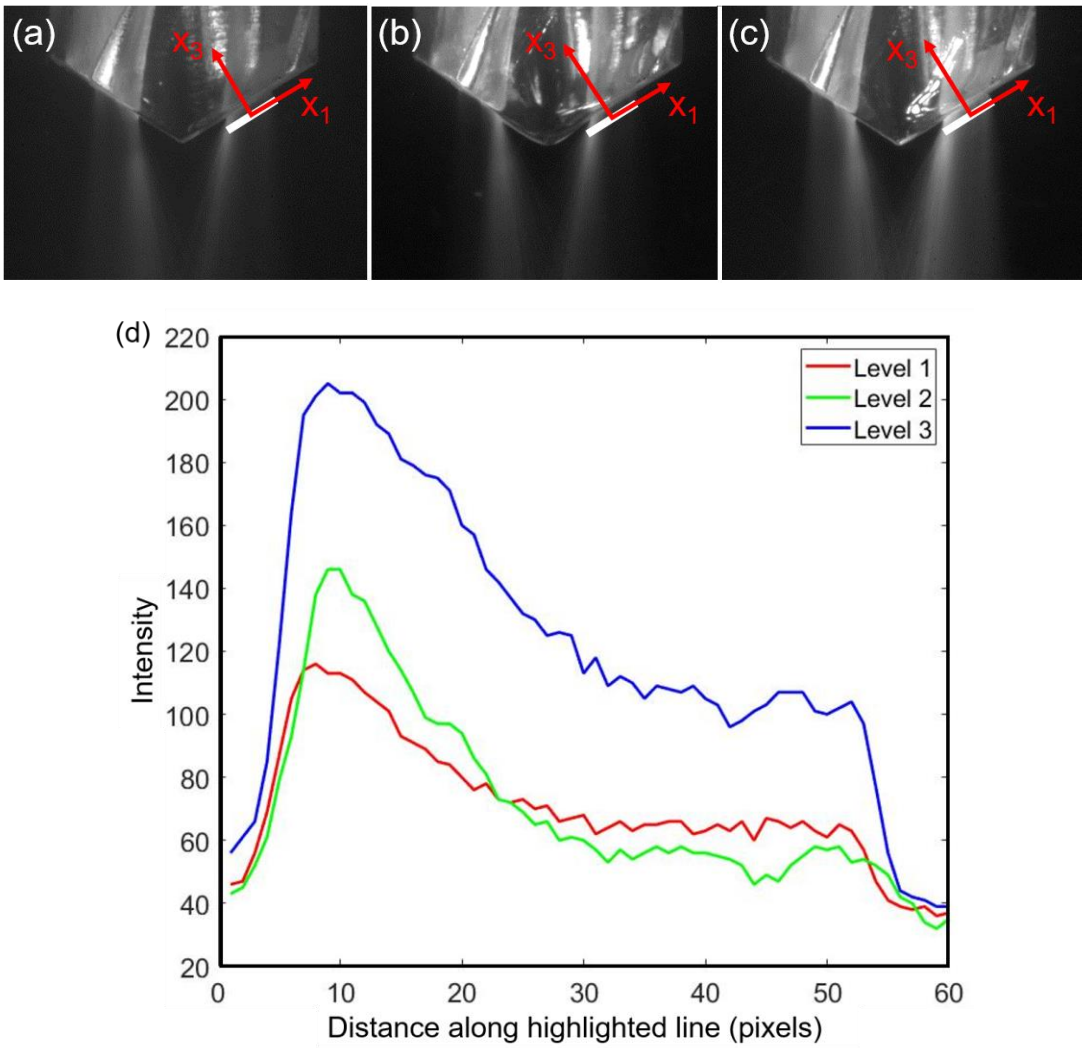

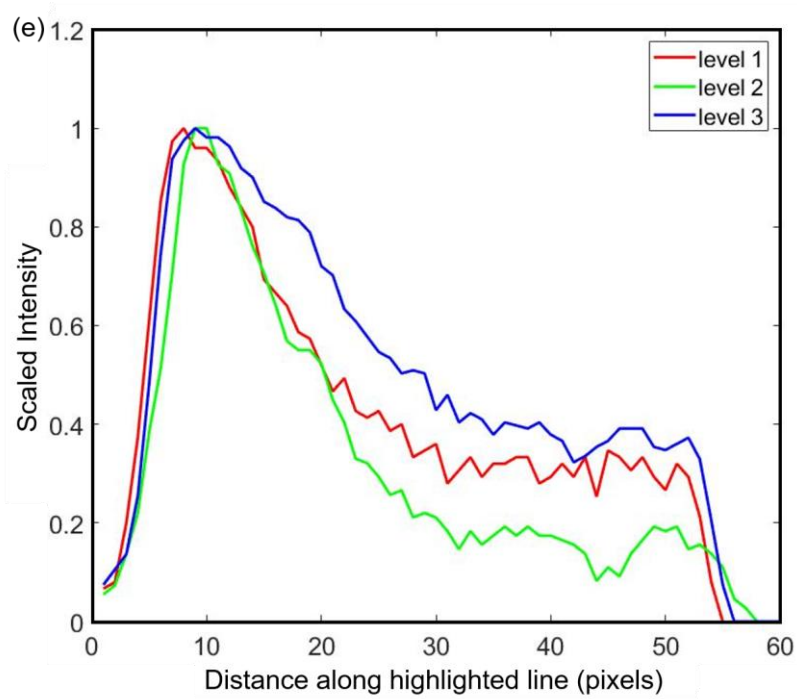

Figure 12: Investigation of irradiance on the flow distribution. (a) Image captured at level 1 intensity (b) Image captured at level 2 intensity (c) Image captured at level 3 intensity (d) Raw intensity profile (e) Scaled intensity profile

generated. Bright LED light sources were used for providing irradiance. The intensity levels were manipulated by varying the distance of the lights from the control volume. Fig. 12(a),(b) & (c) shows the image captured at different level intensities and fig. 12(d) shows the raw intensity profiles obtained along the highlighted line. The results show that the intensity of pixel increases as the irradiance increases. Moreover, it is also observed that the profiles do not align with the x axis, because of light being reflected from other objects in the room. This error is termed as noise. Noise is removed from the profile by subtracting the smallest value of the profile from all the data points. This aligns the profile to the x axis. Now, to eliminate the effect of irradiance from the profile, the profiles are scaled to a scale of 0 to 1 and the results can be seen in fig. 12(e). The result obtained is

called as scaled intensity. The results show that the profiles have a similar magnitude and trend. Thus it was concluded the effect of irradiance can be removed when the profiles are scaled.

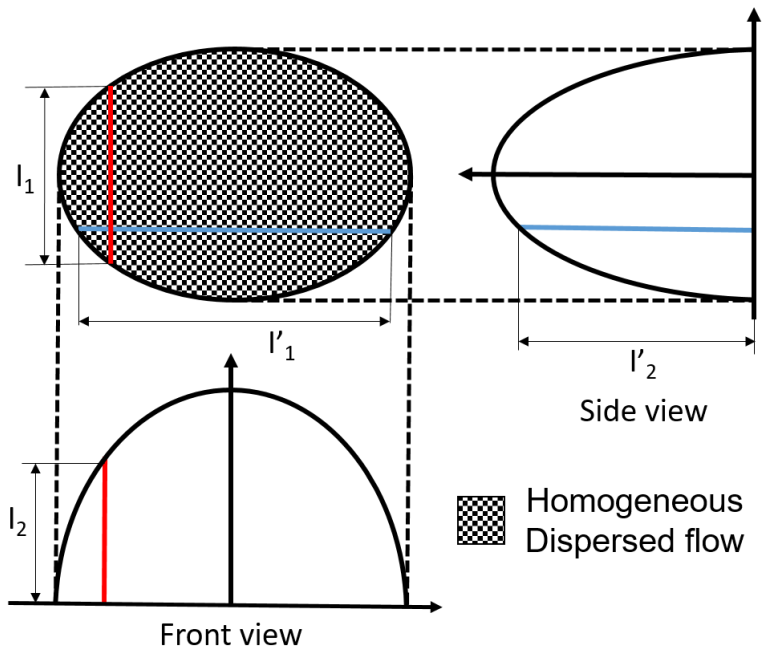

Figure 13: Generation of ideal profile for homogeneous dispersed / mist flow.

The profiles obtained are a superimposition of flow at multiple planes at different depths. Unless the width of the channel is constant no direct conclusion can be made about the distribution of the flow. Therefore the effect of channel shape should be removed from the profile. To eliminate this effect ideal profiles assuming completely homogenous distribution of flow i.e. mist / homogeneous dispersed flow was used as a reference. Reference profile for dispersed flow was used to find the deviation of the actual flow from ideal flow. As can be seen in the fig. 13, the intensity of the pixel is proportional to the no of droplets in the particular direction. This relation can be used to generate ideal profiles.

Value of I_1 is proportional to the value of I_1' and the value of I_2 is proportional to the value of I_2'. To obtain the ideal profile radon transform was used. The radon transform is a common function used in tomography techniques like CT scan, X-ray imaging and MRI as shown in fig. 14.

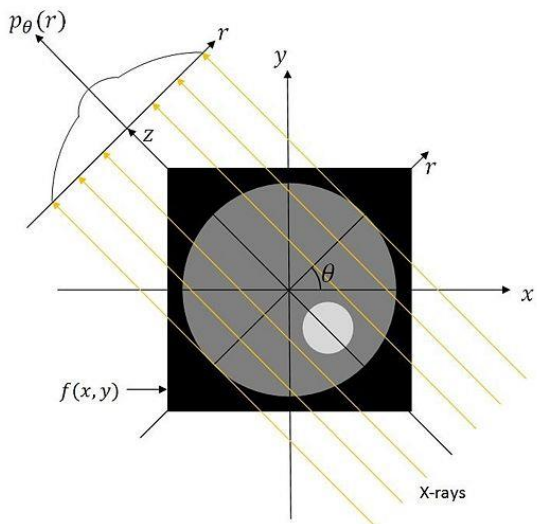

$$z = x * \cos\alpha + y * \sin\alpha$$

$$R(z) = \int_0^l I(r)\, dr$$

Figure 14: Radon transform.

The ideal profiles generated using radon transform were scaled in such a manner that the area under the curve for ideal profile is the same as the area under the curve for the experimentally obtained profile. This was performed to ensure that both the profiles depict the same flow rate. Then the scaled ideal profile was subtracted from the experimentally obtained profile. The new profile obtained is termed as normalized profile, because the effect of intensity as well as the effect of shape of the channel has been eliminated. Positive values indicate high flow concentration zone and negative values indicate low flow concentration zone.

3. EXPERIMENTAL RESULTS

3.1. Design of Experiments

The motive of the study is to look for the effect of helix angle and channel shape on the exit flow structure. Since the drilling operation has very low access to the cutting zone, the exit flow structure has critical importance on the coverage of the cutting fluid on the cutting edge. To evaluate the effect of helix angle and channel shape a full factorial design of experiment was used. Two most commonly available channel shape i.e. circular channel and triangular channel were used and three levels of helix angles i.e. 0, 30 and 45°s were used. Table 2 shows the design of experiment developed to analyze the flow distribution.

	Circular channel	Triangular Channel	Reversed triangular channel
0° helix angle			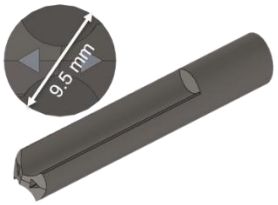
30° helix angle	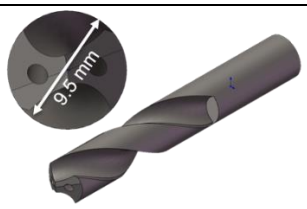		Not Analyzed
45° helix angle	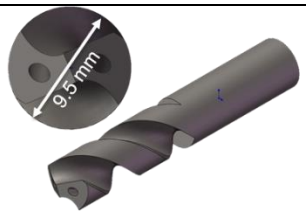		Not Analyzed

Table 2: Design of experiments

To understand if the orientation of channel has an effect on the flow distribution an extended study was conducted with the triangular channel. A channel where the triangular channel is rotated by 180° is designed and named as reversed triangular channel. The design of drills is based on available drills in the market. It is to be noted that the helix angle used to identify the drills, are the helix angle of the drills and not the channels. The pitch of the fluid channel and drill are the same and thus the helix angle of the channel is different from the helix angle of the drill as can be seen in fig. 15.

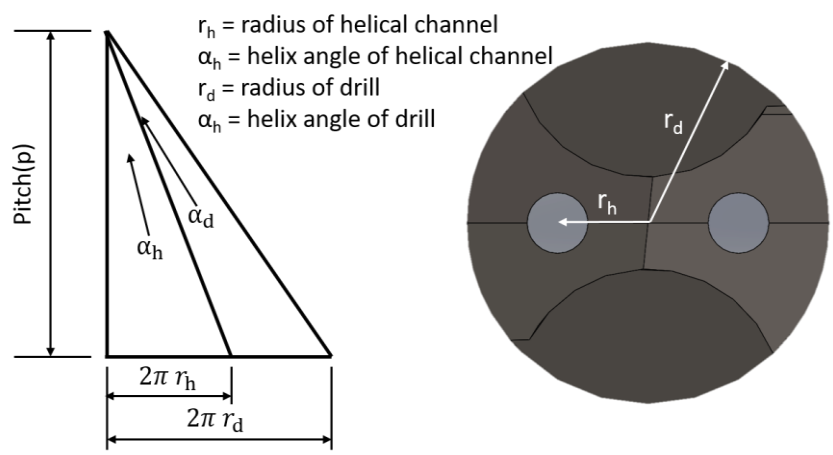

Figure 15: Change in the helix angle of the drill and the helical channel.

A single view of the channel does not provide enough data to be able to map the flow concentration zones across the exit area. Therefore, three viewing angles were decided to better capture the flow distribution and thus provide better prediction. They are named as 0° viewing angle, 45° viewing angle and 90° viewing angle. Fig. 16 shows the exit area for a 0 helix angle circular channel with the viewing direction for all the viewing angles.

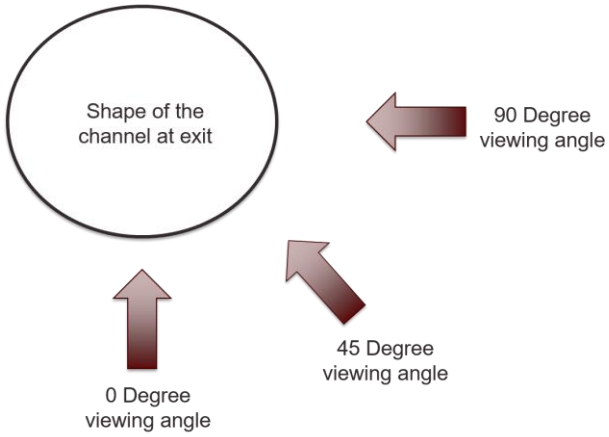

Figure 16: Viewing angles used to capture the flow from multiple angles.

3.2. 0° Helix Angle Circular Channel

As explained previously the image processing method is applied to generate the normalized profile which provides the regions with high and low flow concentrations. Image acquisition is done at three viewing angles and the image processing method is applied to all the cases. Since MQL provides a pulsed flow the flow concentration is not the same at all times. But it is evident that most of the cutting fluid delivery occurs when the flow rate is maximum. Therefore, five frames having maximum flow rate were analyzed and averaged to ensure repeatability. When the drills are rotated to 45° viewing angle and 90° viewing angle, there will be overlap of flow from both the fluid channels. Therefore, to avoid this overlap, one of the channels was closed for all the experiments.

3.2.1. Results for 0°, 45° and 90° Viewing Angle

The camera was aligned as shown in fig. 17(a) and the view observed by the camera is shown in fig. 17(b).

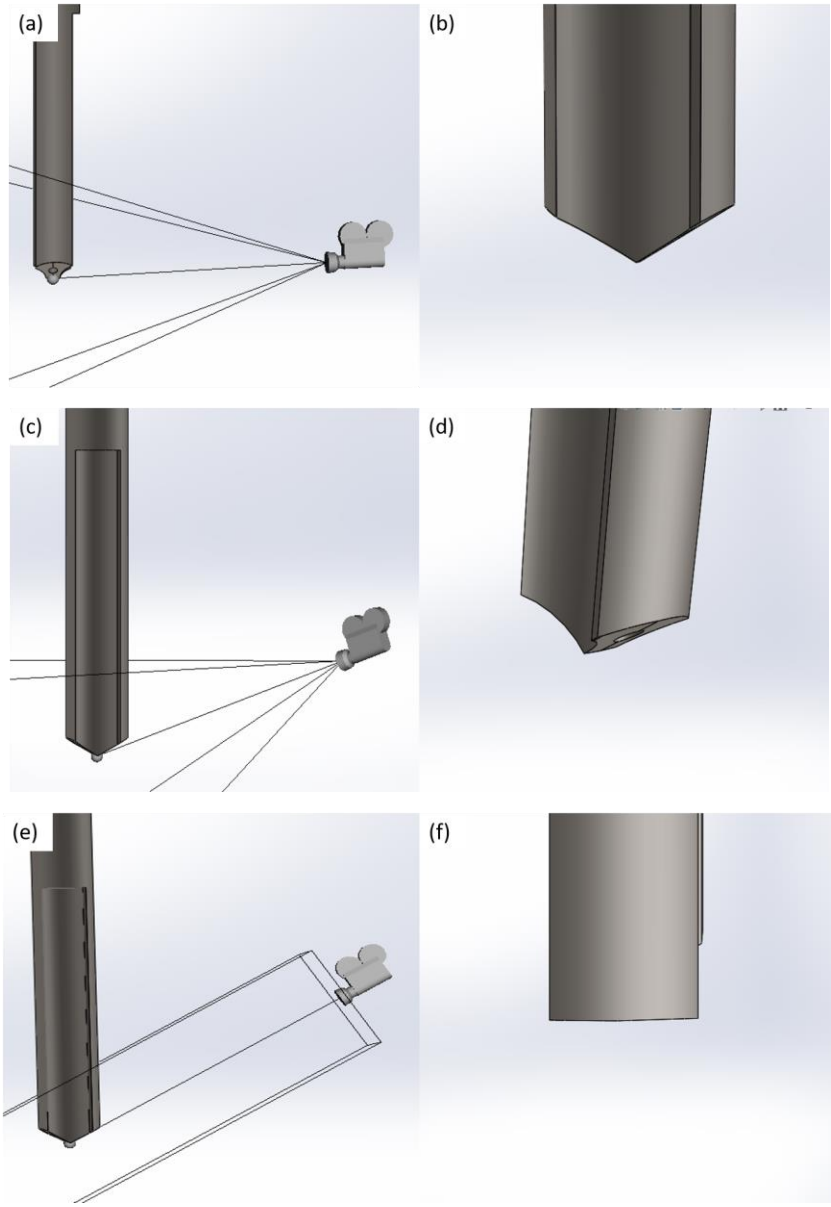

Figure 17: Position and orientation of camera for different viewing angles. (a) Relative position of camera and drill for 0° viewing angle (b) View as seen through the camera for 0° viewing angle (c) Relative position of camera and drill for 45° viewing angle (d) View as seen through the camera for 45° viewing angle (e) Relative position of camera and drill for 90° viewing angle (b) View as seen through the camera for 90° viewing angle

In fig. 18(a) the exit area shape of the channel is shown. The arrow inside the image shows the viewing direction. Radon transform is used to create the theoretical fluid flow

distribution profile as seen in fig. 18(b). Fig. 18(d) shows a sample image captured for the particular case. The highlighted line on the image shows the line along which the intensities are plotted. Fig. 18(e) shows the profiles obtained for different frames and the average profile. As it can be seen that the profiles do not align with the x axis, that is because of the light reflected from other objects in room termed as noise. The noise is removed from the data by subtracting minimum data value from all the data points. After removing the noise we obtain the filtered profile as shown in fig. 18(f). Now the filtered profile is scaled to a range of 0 to 1 and the scaled profile is obtained as seen in fig. 18(g). Since, the area under the scaled profile represents the mass flow rate, the plot in fig. 18(c) is scaled in such a manner that the area under the curve in fig. 18(c) and fig. 18(g) is the

same. Later, the scaled ideal profile (fig. 18(c)) is subtracted from scaled experimental profile (fig. 18(g)) to obtain the normalized profile shown in fig. 18(h).

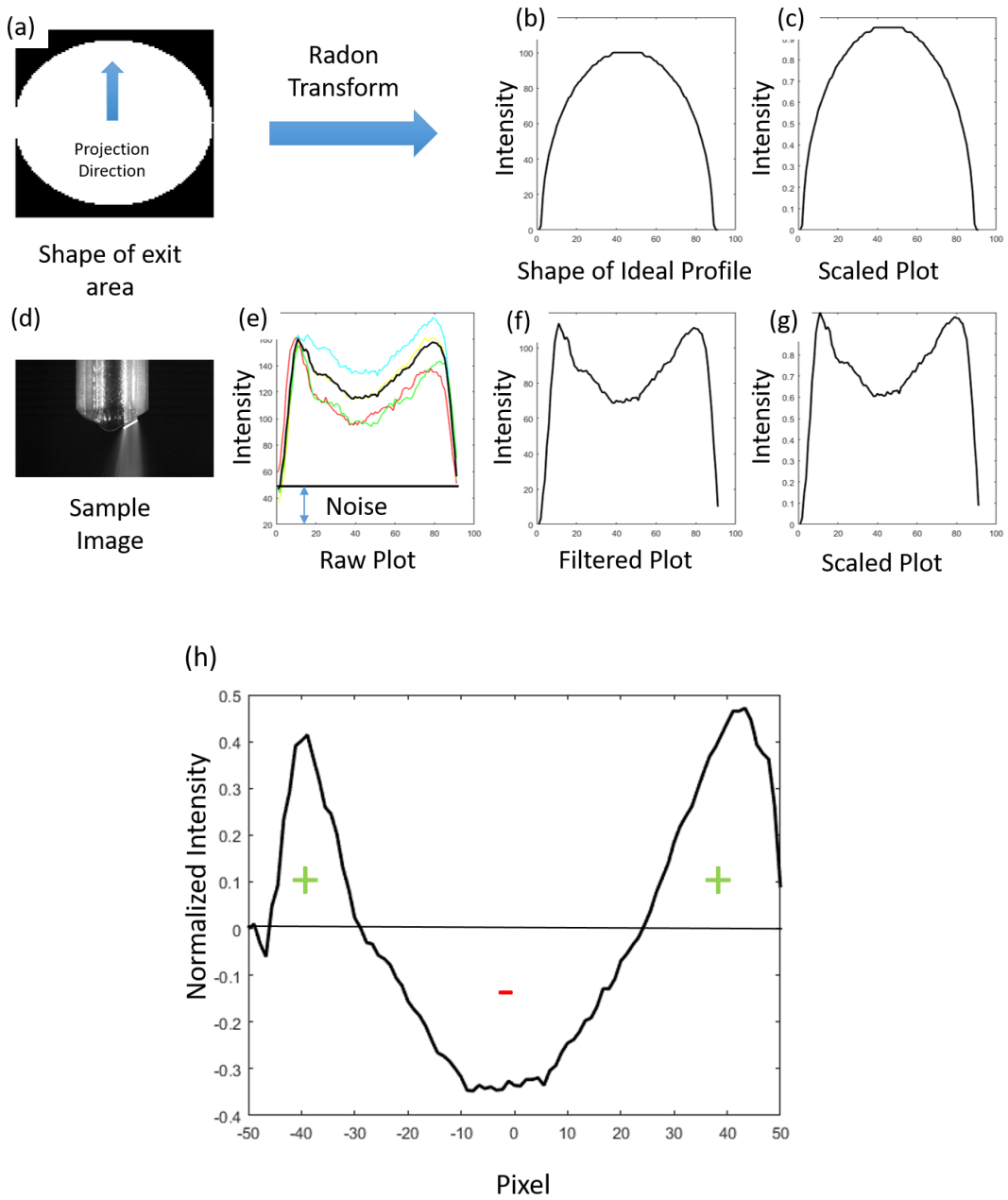

Figure 18: Step by step image processing for 0° helix angle circular channel drill at 0° viewing angle.

It was observed that the flow concentrates towards the edges of the channel. On the left side of the plot a small region with lower flow concentration was seen, that is obtained because of the expansion of flow after coming out of the channel. Same image processing method is applied to other cases. The following are the results obtained for 45 and 90° viewing angle.

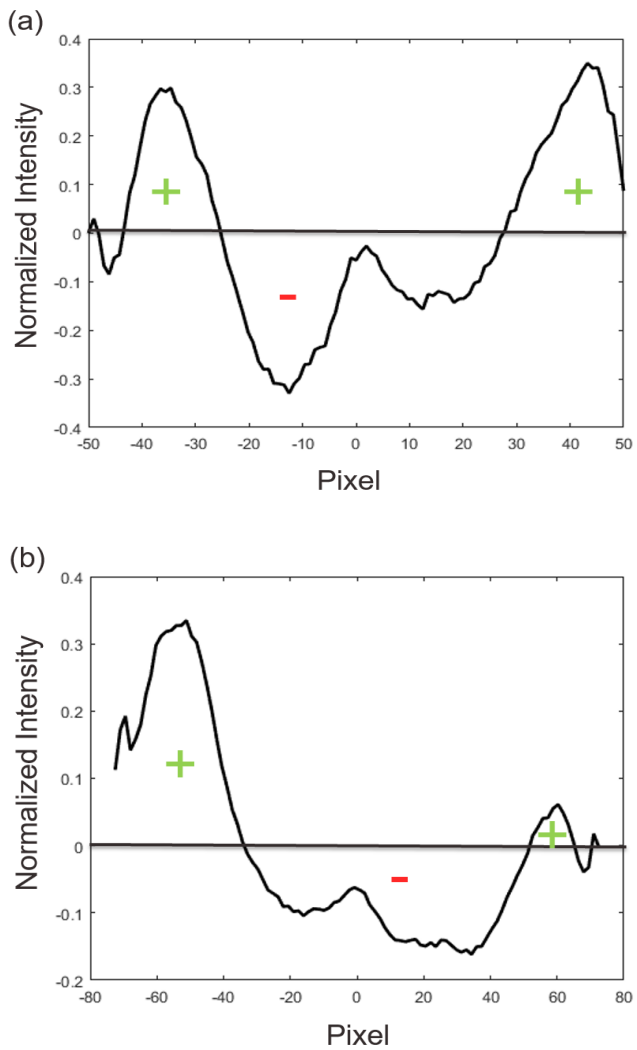

Figure 19: Normalized profiles for 0° helix angle circular channel. (a) 45° viewing angle (b) 90° viewing angle

Similar to the results obtained for 0° viewing angle, the 45 and 90° viewing angles also show flow concentration zones towards the edges of the channel with only exception being the back side of the channel as seen in fig. 19(c) where the flow concentration is close to ideal case.

3.2.2. Flow Mapping Using the Normalized Profiles

The normalized profiles provide information of about flow concentration zones for each viewing angle. To obtain any conclusions about the flow concentration data, the normalized profiles are mapped back to the exit area. It is to be noted that the mapping does not specify the exact oil concentration zones; it only tells that the probability of oil droplets being concentrated on the periphery is higher other locations. It can be observed from the plot that the probable high flow concentration zone is towards the periphery of the channel. Thus the flow falls under the domain of annular flow.

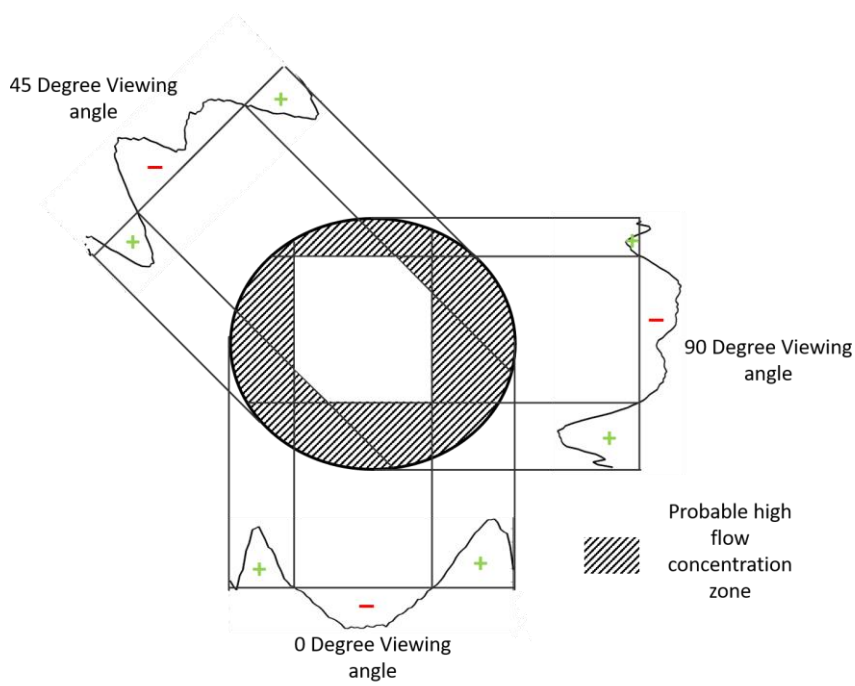

Figure 20: Mapping the projections back on the exit area.

3.3. Results for 30° and 45° Helix Angle Circular Channel

The image processing method explained beforehand was applied to 30° helix angle circular channel case. However, it is to be noted that the exit area is still an ellipse but rotated by about 30° due to the effect of helix angle. The following are the normalized profile obtained for all the viewing angles followed by the area mapping.

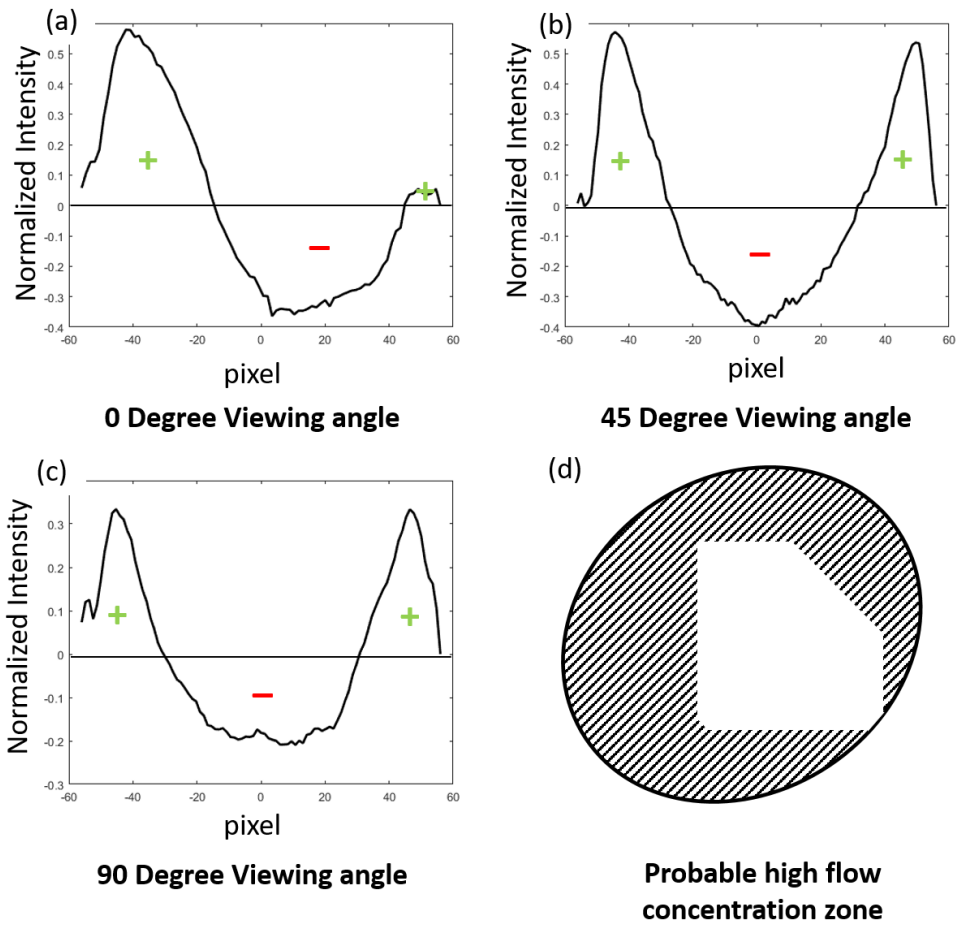

Figure 21: Results for 30° helix angle circular channel. (a) Normalized profile for 0° viewing angle (b) Normalized profile for 45° viewing angle (c) Normalized profile for 90° viewing angle (d) High flow concentration zones mapped back to exit area

As can be seen for 0° viewing angle (fig. 21(a)) there is more flow concentration towards the left side of the channel and the right side being close to ideal flow. The center region of the channel has low flow concentration. From 45° viewing angle (fig. 21(b)), the flow distribution is symmetric about the center of the channel with high concentration towards the edges and low concentration in the center. A similar trend is seen for 90° viewing angle (fig. 21(c)), where high flow concentration towards the edges and low flow concentration at the center is observed. Fig. 21(d) shows the mapping of the flow back to the exit area using the same process as shown in fig. 20. The flow concentration zone is still annular type however, a wider high flow concentration zone is found towards the left side of the area. This means that there is more flow towards the chisel edge of the channel.

The following are the results obtained after experimentation and image processing for 45° helix angle circular channel. It is to be noted that just like 30° helix angle channel, here also the exit area is an ellipse which is rotated by about 45°s. As can be seen for 0° viewing angle (fig. 22(a)) the flow concentration is more on the left side of the channel and a small high flow concentration region on the right side of the channel. The 45° viewing angle (fig. 22(b)) and 90° viewing angle (fig. 22 (c)) shows a similar trend with high flow concentration zones near the edges and low flow concentration zone at the center. When the flow are mapped back onto the area, an annular sort of flow is obtained. However, the core shifts towards left thus making a wider high flow concentration zone towards the left.

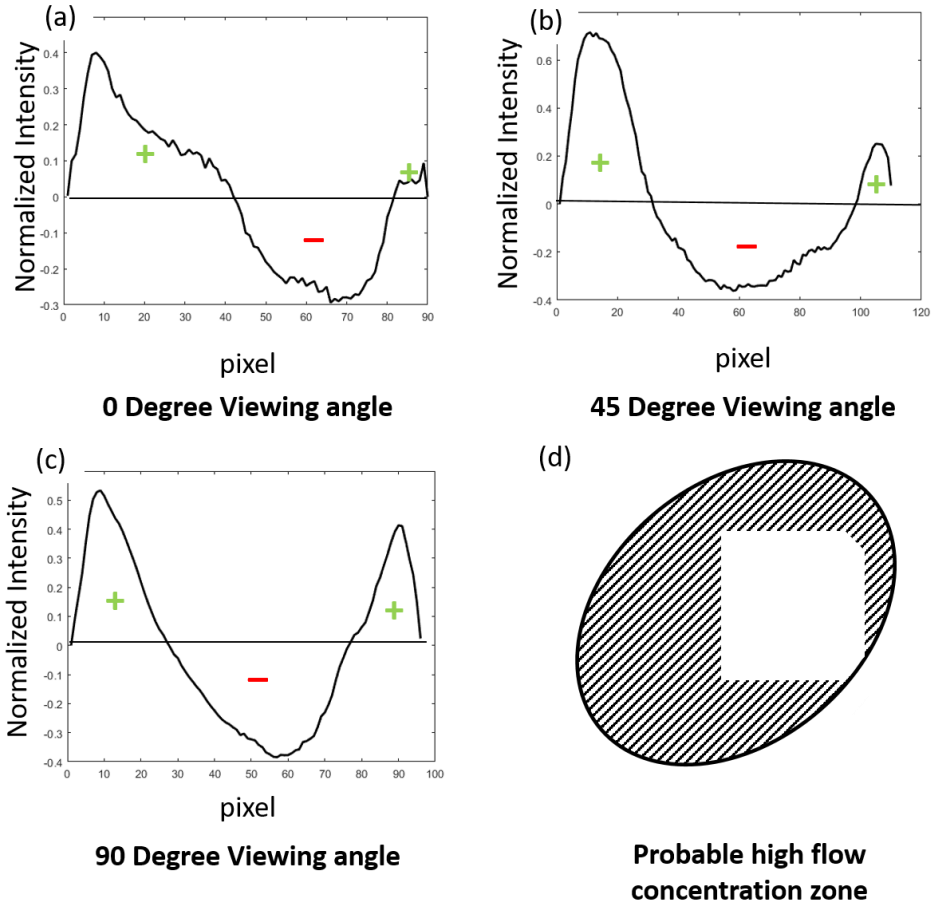

Figure 22: Results for 45° helix angle circular channel. (a) Normalized profile for 0° viewing angle (b) Normalized profile for 45° viewing angle (c) Normalized profile for 90° viewing angle (d) High flow concentration zones mapped back to exit area

3.4. Results for Triangular Channels

The results obtained for a 0 helix angle triangular channel are shown in fig. 23. The 0° viewing angle (fig. 23(a)) shows that the flow concentration is higher than ideal on the left side of the channel i.e. near the chisel edge and low on the right side of the channel. The profile becomes positive near the extreme right of the channel but the width is too small to be taken into consideration. The 45° viewing angle shows that the flow is higher

at the two ends on the channel and lower in the center. And a similar strand is observed for 90° viewing angle as can be seen in fig. 23(c). Fig. 23(d) shows the probable high flow concentration zones, the flow is concentrated at the three vertices of the triangular channel. The flow is annular kind of flow with a low flow concentration in the center and high flow concentration near the periphery of the channel.

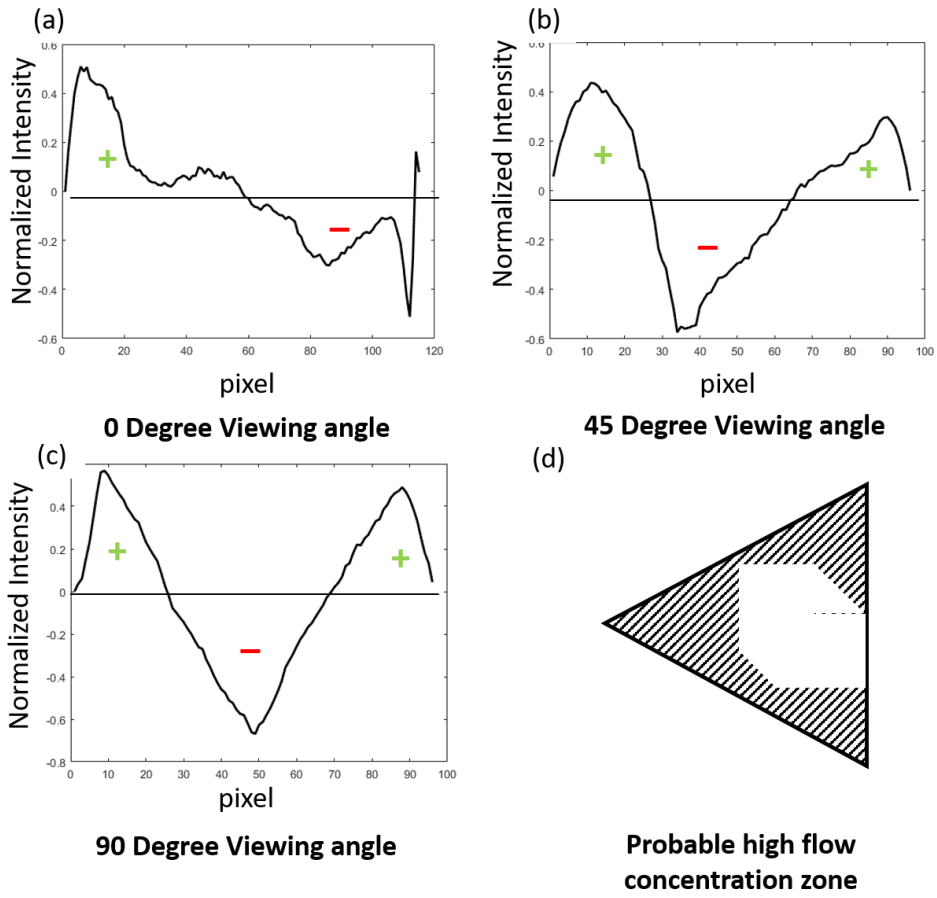

Figure 23: Results for 0° helix angle triangular channel. (a) Normalized profile for 0° viewing angle (b) Normalized profile for 45° viewing angle (c) Normalized profile for 90° viewing angle (d) High flow concentration zones mapped back to exit area

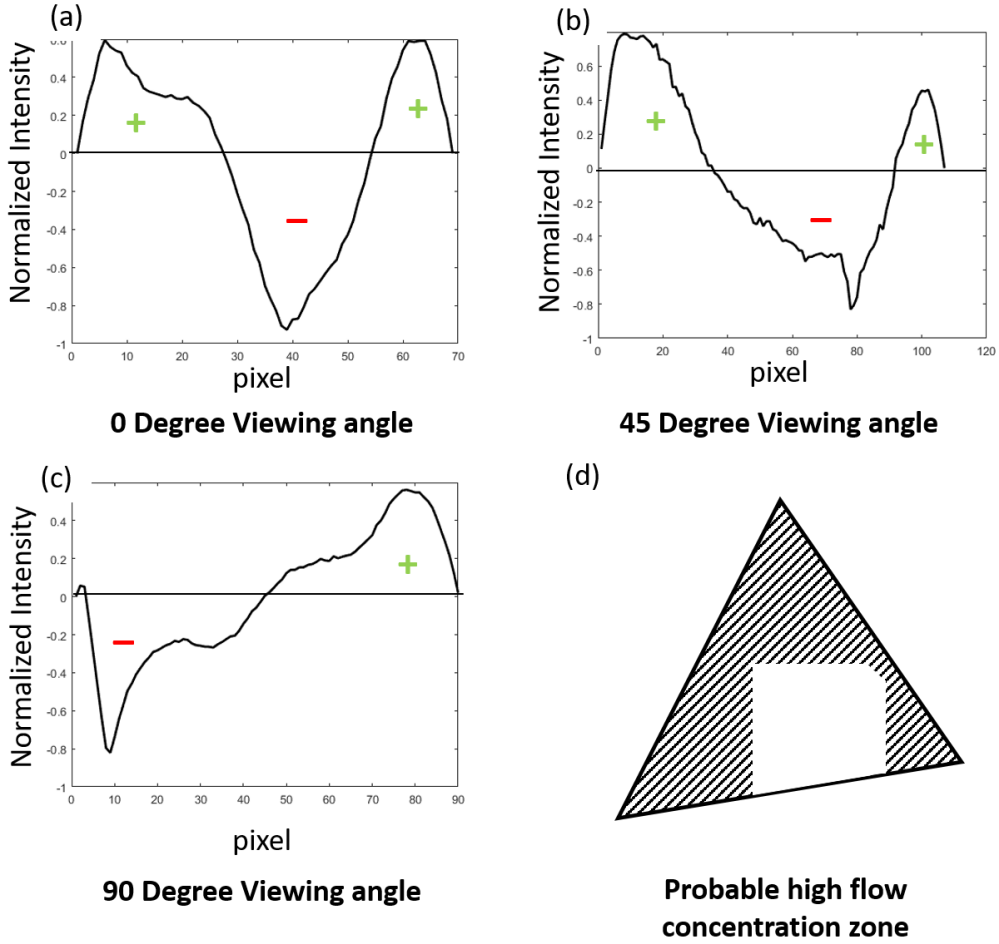

Figure 24: Results for 30° helix angle triangular channel. (a) Normalized profile for 0° viewing angle (b) Normalized profile for 45° viewing angle (c) Normalized profile for 90° viewing angle (d) High flow concentration zones mapped back to exit area

The results obtained for 30 helix angle triangular channel case are shown in fig. 24. The exit area is approximated to be a triangle which is rotated by 30°s because of the helix angle. The 0° viewing angle normalized profile (fig. 24(a)) shows that high flow concentration is obtained at edges of the channel. Different form the 0° helix angle channel, there is a low flow concentration zone in the center region. From fig. 24(b) i.e. 45° viewing angle the trend obtained is similar to the 0° viewing angle high flow

concentration zones at the edges and low flow concentration zone at the center. For 90° viewing angle i.e. fig 24(c), high flow concentration zone is obtained at the rear end of the channel and low flow concentration zone on the front end. When the flow are mapped back onto the area, unlike 30° helix angle circular channel where the low flow concentration core shifted to the right, away from the chisel edge, here the low flow concentration zone shifts toward left / chisel edge.

The results for 45° helix angle triangular channel are shown in fig. 25. It is to be noted that the exit area is a triangle which is rotated by 45°. For 0° viewing angle the normalized profile shows high flow concentration zones at the edges and low flow concentration zone at the central region. The 45° viewing angle shows high flow concentration towards the left i.e. chisel edge of the channel and 90° viewing angle shows that there are high floe concentration zones at the edges and low flow concentration zone in the central region. When the flow is mapped on the exit area it is found that there is central low flow concentration region and high flow concentration at all the vertices. The low flow concentration zone is shifted towards the center of the channel and a little bit towards the chisel edge of the channel.

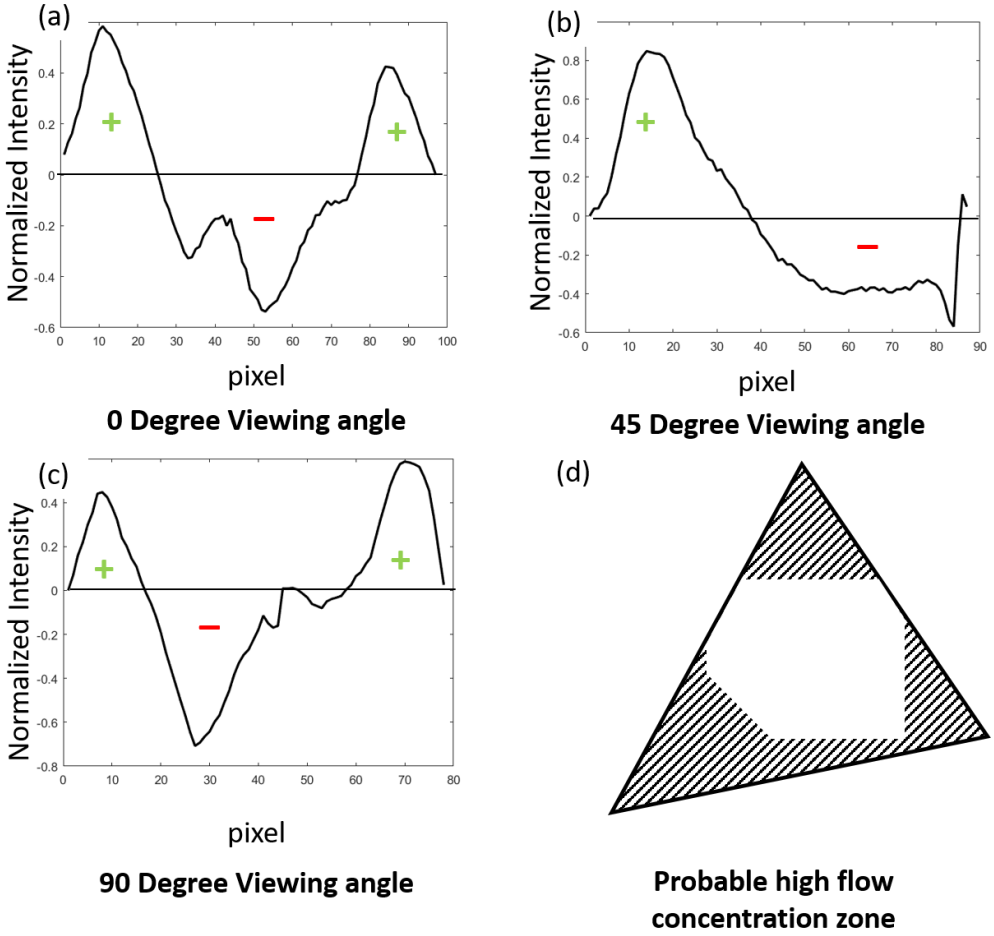

Figure 25: Results for 45° helix angle triangular channel (a) Normalized profile for 0° viewing angle (b) Normalized profile for 45° viewing angle (c) Normalized profile for 90° viewing angle (d) High flow concentration zones mapped back to exit area

3.5. 0° Helix Angle Reversed Triangular Channel

The results are shown in fig. 26. The flow mapping shown is fig 26(d) shows that the probable high flow concentration region is exactly a mirror image of that of a 0 helix angle triangle. This result may be insightful to understand the phenomenon behind the process.

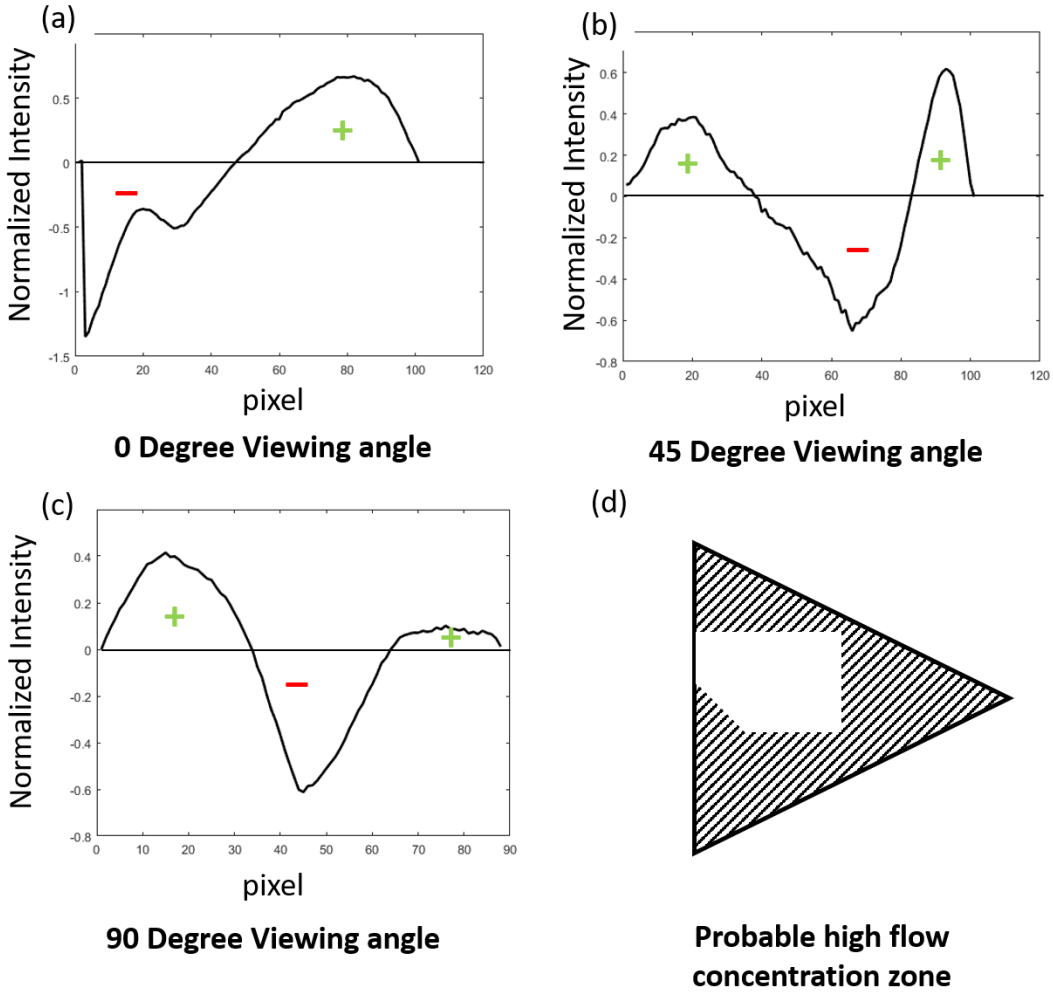

Figure 26: Results for 0° helix angle reversed triangular channel (a) Normalized profile for 0° viewing angle (b) Normalized profile for 45° viewing angle (c) Normalized profile for 90° viewing angle (d) High flow concentration zones mapped back to exit area

4. NUMERICAL SOLUTION

4.1. CFD Model Setup and Boundary Conditions

MQL is a multiphase flow. Fluent module of ANSYS provides a multiphase flow provides multiple models to solve multiphase flow. Two of the most multiphase models are VOF, Eulerian and Mixture model. However, a multiphase simulation requires a mesh size smaller than the size of the particles. For MQL the droplet size can be as small as 5μm[20], therefore the mesh size should be smaller than that to effectively capture the droplet flow. But the channel size are in the order of 1-2 mm and the lengths are in the order of 50 mm, therefore the no of nodes for the mesh size is extremely high. This results in extremely long simulation time and requirement of super computers for solving multiphase problems.

It was hypothesized that in MQL since 99% of the flow is air, the flow of droplets is controlled by the flow of air. Therefore, a single phase simulation was performed using the fluent module in ANSYS. Fig. 27 shows the sample control volume and cross-sectional mesh. To reduce the computational effort and to be better able to capture the boundary layer, inflation was used near the channel periphery. This lead to a smaller mesh size at the periphery and larger mesh size in the core region. According to data provided by Ford Motor Company (Dearborn, MI), the average flow velocity inside the channel can be as high as 290 m/s for a 1-2 mm diameter channel for input pressure of 5.5 bar. The corresponding Reynolds number is over 30000, which means that the flow is highly turbulent. For this, the standard κ-ε model was used. Researchers have developed a simplified single phase model for multiphase flow where, the density of the simulated fluid

is the weighted average of the constituent fluids in multiphase flow. However, in the case of MQL, as stated earlier the volume fraction of oil is negligible as compared to air and thus, properties of air were directly used for simulation purposes. The Mach number at ambient conditions (300K) was calculated to be about 0.8, which is more than 0.3. Hence, compressibility effects need to be accounted for, because, the change in density of the fluid remains no longer negligible. Thus, a density based solver was used. Considering all the above facts, the boundary conditions used were inlet velocity as 290 m/s and exit pressure 1 atm. (zero gauge pressure at the exit). A no-slip boundary condition on the channel wall was assumed.

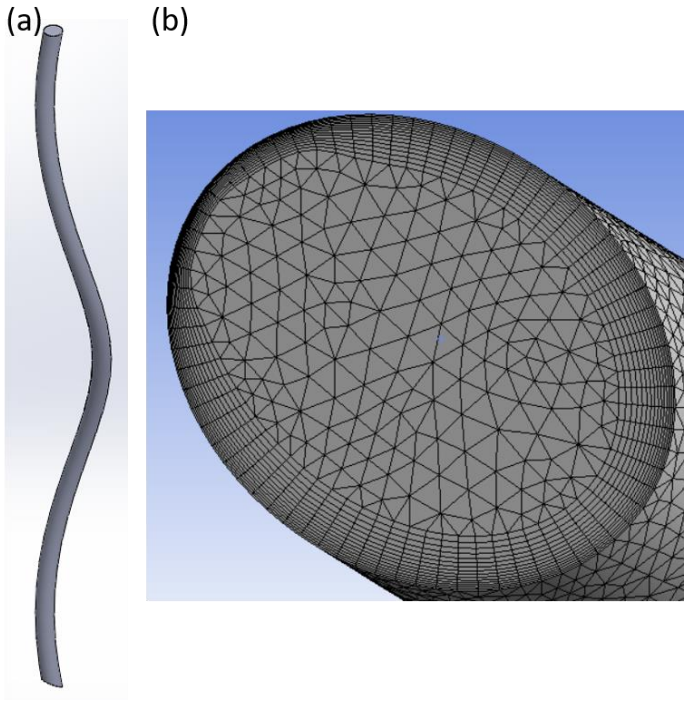

Figure 27: Control volume for simulation. (a) Control volume for a 30° helix angle circular channel (b) Cross-sectional mesh for 30° helix angle circular channel

4.2. Computational Results

The numerical solution was performed for all the cases explained in the design of experiment. It was made sure that the channel length for each case is kept the same, because the length of the channel plays an important role in the development of flow profile.

4.2.1. Solution for Circular Channels

Fig. 28 shows the velocity contours obtained at the exit of channel for a 0° helix angle circular channel. As it can be seen that the flow has a higher velocity in the center and the velocity reduces as we move towards the edges.

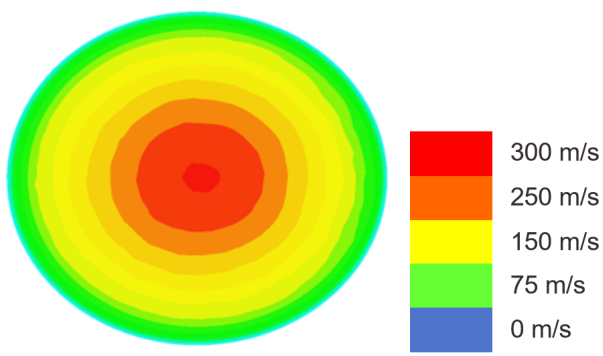

Figure 28: Velocity contours at exit for 0° helix angle circular channel.

Fig. 29 shows the velocity contours obtained at the exit of the channel for a 30° helix angle circular channel. As it can be seen, different from the previous case the flow profile is asymmetric. The high flow velocity region has shifted to the right making a low velocity region near the chisel edge of the drill. This shift is obtained because of the centrifugal forces generated due to motion in a helical path. This solution matches with the solution obtained Yamamoto et al.[29].

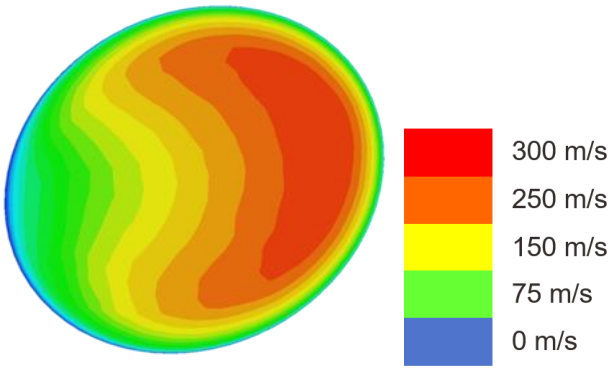

Figure 29: Velocity contours at exit for 30° helix angle circular channel.

Similar to the 30° helix angle circular channel, the flow profile in 45° helix angle circular channel has become even more asymmetric. The high flow velocity region shifted even more away from the chisel edge of the drill and the size of the low velocity region on the left side of the channel even increased as can be seen in fig. 30

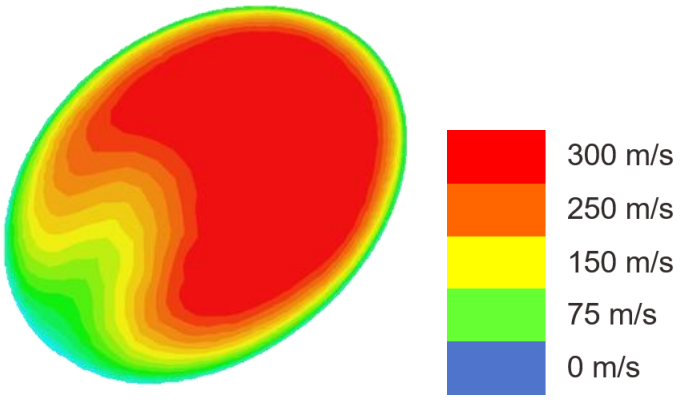

Figure 30: Velocity contours at exit for 45° helix angle circular channel.

4.2.2. Solution for Triangular Channels

Fig. 31 shows the flow contours obtained at the exit of the 0° helix angle triangular channel. While modelling triangular channels, the vertex of the triangles were filleted by a radius of 01.mm. This was done because the drills are made using SLA printer and the resolution of the printer is 0.1mm thus it cannot make sharp internal corners smaller than 0.1mm. Similar to the 0 helix angle circular channel the high flow velocity region is in the center of the channel and low flow velocity region in the periphery.

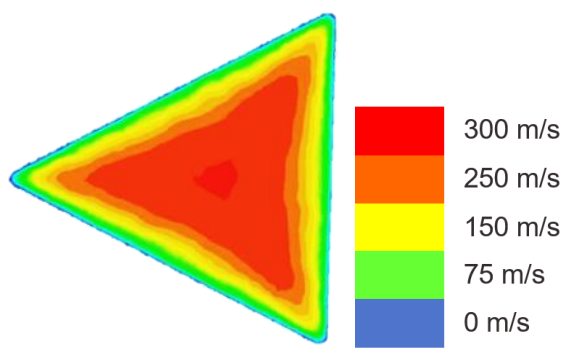

Figure 31: Velocity contours at exit for 0° helix angle triangular channel.

Fig. 32 shows the velocity contours obtained at the exit of the channel for 30° helix angle triangular channel. The high velocity region is still in the center of the drill but there is some evident twisting motion in the flow. This is possible because unlike circular channel the boundary in triangular channel is not equidistant from the center of the channel and thus the fluid starts spinning along the center.

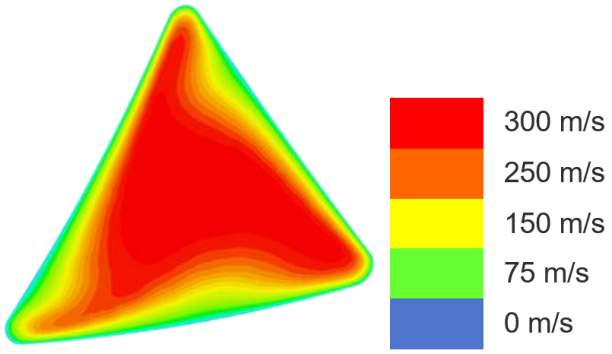

Figure 32: Velocity contours at exit for 30° helix angle triangular channel.

Fig. 33 shows the velocity contours obtained using the numerical solution for 45° helix triangular channel. Similar to the results in 30° helix angle triangular channel, the flow is even more twisted about the center. This means a higher helix angle produces a more severe effect on the flow distribution. If the results are extrapolated to a higher helix angle a high velocity circular zone will be found in the center and low velocity zone will be at the vertex.

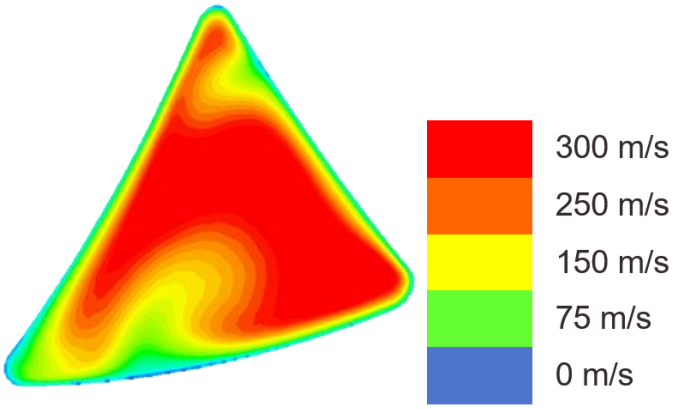

Figure 33: Velocity contours at exit for 45° helix angle triangular channel.

4.2.3. 0° Helix Angle Reversed Triangular Channel

Fig. 34 shows the velocity contours at the exit of the channel. Ass compared to the results obtained for 0° helix angle triangular channel the flow profile is an exact mirror image. This is intuitive because both of them have the same boundary conditions.

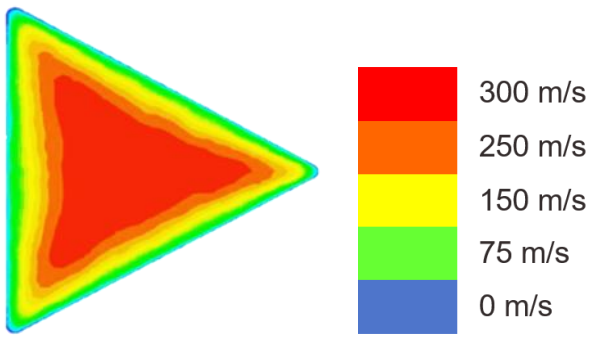

Figure 34: Velocity contours at exit for 0° helix angle reversed triangular channel.

4.3. Comparison of the Results

After completing numerical solutions for each case a correlation is observed between the flow distribution and the velocity. It was observed that the flow distribution is higher in the low velocity region and flow concentration is lower in high velocity region. Table 3 compares the experimental results and the numerical solution by overlaying them on each other. The trend obtained in the flow distribution is similar to the trend obtained in the velocity distribution.

	Circular Channel	Triangular Channel	Reversed triangular channel
0 Helix Angle	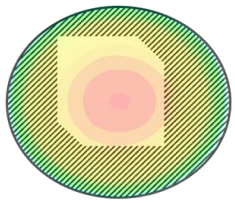	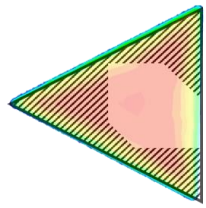	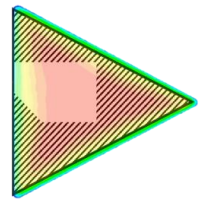
30 Helix Angle	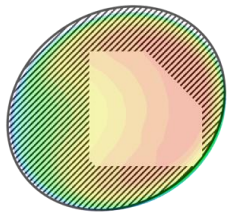	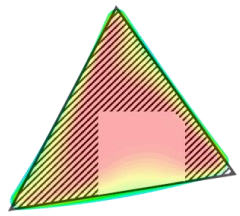	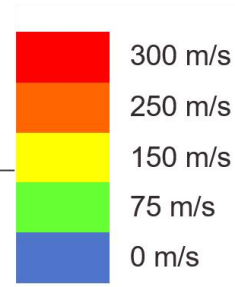
45 Helix Angle	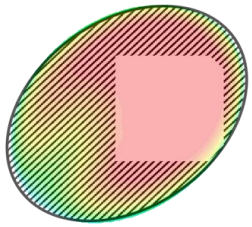	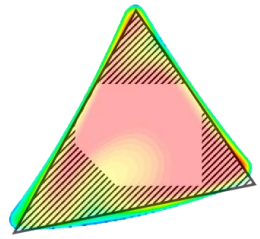	

Table 3: Comparison of experimental results and numerical solution.

As can be seen for all the cases, the low flow concentration zone is always around the high flow velocity zone. This correlation is useful because now the flow distribution can be directly predicted using a single phase simulation rather than approaching the problem using an exhaustive multiphase solution.

5. DISCUSSION, CONCLUSIONS AND FUTURE SCOPE

5.1. Discussion

Form the results it is evident that the oil droplets tend to gather in the low velocity region. This observation can be helpful because a direct relation is observed between the flow distribution and the velocity distribution. One of the possible reasons to justify this behaviour is based upon the loss in energy principle or minimum energy loss principle. Any physical process happens in such a manner that the amount of loss happening during the process are lowered. For example more current will flow to lower resistance path and less current will flow through high resistance path. Applying the same analogy to fluid flow, the resistance is analogous to viscous loss and current is analogous to velocity. Air is less viscous than lubricant and therefore to reduce the amount of energy lost due to viscous forces, air occupies high velocity region and the lubricant droplets are thrown into high shear zones where the velocity is low[30].

Moreover, the contact angles measured for the UNIST CL2210 lubricant with the tool material ranged from 16° to 18° which means the surface energy of the solid (tool material) is higher than that of the liquid (lubricant). Because of the high surface energy, the adhesion forces between the lubricant and drill are high. These high adhesion forces pull the droplet towards the wall of the channel and therefore the droplet density at the channel periphery increases. This can be one of the reasons for obtaining higher droplet concentration at the channel periphery. Both of the aforementioned principles can control the droplet distribution and further investigation is required before making any conclusion about which principle plays a significant role in droplet distribution.

For the case of 0° helix angle circular channel, the flow concentration was obtained higher near the periphery of the channel, which is where low flow velocity is observed. Similarly for the 30° helix angle circular channel, asymmetric velocity profile was generated due to the centrifugal forces acting on the fluid because of the helical path. Therefore a low velocity zone was created on the left side of the channel i.e. near the chisel edge. Moreover, the width of flow concentration zone increases near the chisel edge. Similar situation is obtained for the 45° helix angle circular channel.

For the 0° helix angle triangular channel, the low flow concentration zone is observed in the center of the channel although slightly shifted away from the chisel edge. This result coincides with the numerical result. Also, according to the numerical solution the flow distribution in 0° helix angle triangular channel should be an exact mirror image of the 0° helix angle reversed triangular channel. This prediction matches with the experimental flow distribution obtained for both the cases as the flow distribution across the areas are mirror images of each other.

For the 30 and 45° helix angle triangular channel, the flow distribution shifts towards the center of the channel. This coincides with the velocity profiles, the helix angles in the triangular channel creates a twist in the velocity contours and thus creates a high velocity core in the center of the channel. The intensity of this twist is dependent on the value of helix angle and a higher helix angle produces a more severe distortion.

Limitation of this study is the naturally pulsed flow of MQL system. Despite a high frequency, the mist flow is not a completely continuous stream. Instead, the mass flow rate varies slightly overtime. The normalization can diminish this effect only up to a

certain extent. From the measurement perspective, it is important to synchronize the image acquisition with the flow pulse to ensure that the measurement is always taken at the same mass flow rate.

5.2. Conclusions

Current research was limited to a qualitative analysis of flow distribution and therefore no quantitative conclusions can be made. However, the findings of the research provide an insight on the physics behind the flow distribution in multiphase flows like MQL. The following are the conclusions:

1. The proposed method which uses amount of light reflected from the control volume as a signal for determining the flow distribution, can be used to map the flow distribution across the channels.
2. The irradiance, light orientation and ambient light all have an effect on the flow profile generated.
3. Channel shape, helix angle and orientation all have an effect on the flow distribution.
4. The flow distribution in MQL is dependent on the velocity distribution of air in the channel.
5. The adhesion between the tool and the workpiece plays a critical role in determining the flow distribution.

5.3. Future Scope

The main limitation of the study is, a quantitative comparison is required between the flow distribution and the velocity contours. To counter this limitation tomography

methods inspired form MRI, X-ray scanning and CT can be used to generate a quantitative distribution of the flow in the channel. Moreover, according to the literature, the back pressure generated by the workpiece also affects the flow distribution on the channel. This effect can be analyzed to quantify the hypothesis presented by multiple researchers. Lastly, the flow measurement can be done at different cross-sections in the channel to study the flow development as the flow passes through the channel.

REFERENCES

[1] Wong, K. V., and Hernandez, A., 2012, "A review of additive manufacturing," ISRN Mechanical Engineering, 2012.

[2] Bruni, C., Forcellese, A., Gabrielli, F., and Simoncini, M., 2006, "Effect of the lubrication-cooling technique, insert technology and machine bed material on the workpart surface finish and tool wear in finish turning of AISI 420B," International Journal of Machine Tools and Manufacture, 46(12), pp. 1547-1554.

[3] Tai, B. L., Stephenson, D. A., and Shih, A. J., 2012, "An Inverse Heat Transfer Method for Determining Workpiece Temperature in Minimum Quantity Lubrication Deep Hole Drilling," Journal of Manufacturing Science and Engineering, 134(2), pp. 021006-021006-021008.

[4] Raynor, P. C., Kim, S. W., and Bhattacharya, M., 2005, "Mist generation from metalworking fluids formulated using vegetable oils," Annals of Occupational Hygiene, 49(4), pp. 283-293.

[5] Filipovic, A., and Stephenson, D. A., 2006, "Minimum Quantity Lubrication (MQL) applications in automotive power-train machining," Machining Science and Technology, 10(1), pp. 3-22.

[6] Heinemann, R., Hinduja, S., Barrow, G., and Petuelli, G., 2006, Effect of MQL on the tool life of small twist drills in deep-hole drilling.

[7] Lerma, I., Jimenez, M., Edinbarough, I., Krell, J., and Hung, N. P., 2015, "Characterization of Micromist for Effective Minimum Quantity Lubrication," Advanced Materials Research, 1115, pp. 43-46.

[8] Tai, B. L., Jessop, A. J., Stephenson, D. A., and Shih, A. J., 2012, "Workpiece Thermal Distortion in Minimum Quantity Lubrication Deep Hole Drilling—Finite Element Modeling and Experimental Validation," Journal of Manufacturing Science and Engineering, 134(1), pp. 011008-011008-011009.

[9] Vivek, T. G., Vikas, T. P., Kuppan, P., Balan, A. S. S., and Oyyaravelu, R., 2016, "Experimental investigation of machining parameter under MQL milling of SS304," IOP Conference Series: Materials Science and Engineering, 149(1), p. 012023.

[10] Tai, B. L., Stephenson, D. A., Furness, R. J., and Shih, A. J., 2014, "Minimum Quantity Lubrication (MQL) in Automotive Powertrain Machining," Procedia CIRP, 14, pp. 523-528.

[11] Kuzu, A. T., Berenji, K. R., Ekim, B. C., and Bakkal, M., 2017, "The thermal modeling of deep-hole drilling process under MQL condition," Journal of Manufacturing Processes, 29, pp. 194-203.

[12] Le Coz, G., Marinescu, M., Devillez, A., Dudzinski, D., and Velnom, L. J. A. T. E., 2012, "Measuring temperature of rotating cutting tools: Application to MQL drilling and dry milling of aerospace alloys," 36, pp. 434-441.

[13] Tawakoli, T., Hadad, M., and H. Sadeghi, M., 2010, Influence of oil mist parameters on minimum quantity lubrication – MQL grinding process.

[14] Davim, J., Sreejith, P. S., and Silva, J., 2007, Turning of Brasses Using Minimum Quantity of Lubricant (MQL) and Flooded Lubricant Conditions.

[15] Attanasio, A., Gelfi, M., Giardini, C., and Remino, C., 2006, "Minimal quantity lubrication in turning: Effect on tool wear," Wear, 260(3), pp. 333-338.

[16] Li, Q., Lerma, I., Alvarado, J., Edinbarough, I., and Hung, W. N. P., 2015, "Characterization of Micromist for Effective Machining," (57359), p. V02AT02A058.

[17] Chen, M., Jiang, L., Shi, B. W., Liu, Z. Q., and An, Q. L., 2012, "CFD Analysis on the Flow Field of Minimum Quantity Lubrication during External Thread Turning," Materials Science Forum, 723, pp. 113-118.

[18] Sharma, A. K., Tiwari, A. K., and Dixit, A. R., 2016, "Effects of Minimum Quantity Lubrication (MQL) in machining processes using conventional and nanofluid based cutting fluids: A comprehensive review," Journal of Cleaner Production, 127, pp. 1-18.

[19] Tasdelen, B., Wikblom, T., and Ekered, S., 2008, "Studies on minimum quantity lubrication (MQL) and air cooling at drilling," Journal of Materials Processing Technology, 200(1), pp. 339-346.

[20] A. Khan, W., M. Hoang, N., Tai, B., and N.P. Hung, W., 2018, Through-tool minimum quantity lubrication and effect on machinability.

[21] Rahim, E. A., and Dorairaju, H., 2018, "Evaluation of mist flow characteristic and performance in Minimum Quantity Lubrication (MQL) machining," Measurement, 123, pp. 213-225.

[22] Sovani, S. D., Chou, E., Sojka, P. E., Gore, J. P., Eckerle, W. A., and Crofts, J. D., 2001, "High pressure effervescent atomization: effect of ambient pressure on spray cone angle," Fuel, 80(3), pp. 427-435.

[23] Husted, B. P., Petersson, P., Lund, I., and Holmstedt, G., 2009, "Comparison of PIV and PDA droplet velocity measurement techniques on two high-pressure water mist nozzles," Fire Safety Journal, 44(8), pp. 1030-1045.

[24] Park, K.-H., Olortegui-Yume, J., Yoon, M.-C., Kwon, P. J. I. J. o. M. T., and Manufacture, 2010, "A study on droplets and their distribution for minimum quantity lubrication (MQL)," 50(9), pp. 824-833.

[25] Falcone, G., Hewitt, G., and Alimonti, C., 2009, Multiphase flow metering: principles and applications, Elsevier.

[26] Maruda, R. W., Krolczyk, G. M., Feldshtein, E., Pusavec, F., Szydlowski, M., Legutko, S., and Sobczak-Kupiec, A., 2016, "A study on droplets sizes, their distribution and heat exchange for minimum quantity cooling lubrication (MQCL)," International Journal of Machine Tools and Manufacture, 100, pp. 81-92.

[27] Tai, B. L., Dasch, J. M., and Shih, A. J., 2011, "Evaluation and comparison of lubricant properties in Minimum Quantity Lubrication machining," Machining Science and Technology, 15(4), pp. 376-391.

[28] Dasch, J., and Kurgin, S., 2010, "A characterisation of mist generated from minimum quantity lubrication (MQL) compared to wet machining,"International journal of Machining and Machinability of Materials, 7(1), pp. 82-95.

[29] Yamamoto, K., Alam, M. M., Yasuhara, J., and Aribowo, A., 2000, "Flow through a rotating helical pipe with circular cross-section," International Journal of Heat and Fluid Flow, 21(2), pp. 213-220.

[30] Brennen, C. E., and Brennen, C. E., 2005, Fundamentals of multiphase flow, Cambridge University Press.